Issues in the Design of Shape Memory Alloy Actuators

by

Stéphane Lederlé

Diplôme d'Ingénieur ENSTA - Paris (FRANCE), 2002

Submitted to the Department of Aeronautics and Astronautics
in partial fulfillment of the requirements for the degree of Master of Science in Aeronautics and Astronautics

at the

MASSACHUSETTS INSTITUTE OF TECHNOLOGY

June 2002

Author .....
Department of Aeronautics and Astronautics
May 23, 2002

Certified by .....
Steven R. Hall
Professor of Aeronautics and Astronautics
Thesis Supervisor

Accepted by .....
Wallace E. Vander Velde
Professor of Aeronautics and Astronautics
Chair, Committee on Graduate Students

Issues in the Design of Shape Memory Alloy Actuators

by

Stéphane Lederlé

Submitted to the Department of Aeronautics and Astronautics
on May 23, 2002, in partial fulfillment of the
requirements for the degree of
Master of Science in Aeronautics and Astronautics

Abstract

This thesis considers the application of shape memory alloy (SMA) actuators for shape control of the undertray of a sports car. By deforming the shape of the structure that provides aerodynamic stability to the car, we expect to improve the overall performance of the vehicle by adapting its aerodynamics according to the vehicle speed. We then develop a methodology for designing SMA actuators in this application. The methodology is based on the integration of the different models involved: mechanical, thermal, and electrical. The constraints imposed on the device are also incorporated. Unfortunately, the analysis predicts an actuation time that is too slow for this particular application. Still, we use our assembled model to sketch the expected characteristics of SMA actuators. A significant result is that the actuation time is a function of the amount of energy the active material has to provide, and that there is a necessary trade-off between the mass of actuators and the actuation time. In particular, the expected energy density may have to be decreased to achieve acceptable actuation times. Finally, we propose a way to estimate *a priori* the suitability of SMA actuators for a particular application.

Thesis Supervisor: Steven R. Hall
Title: Professor of Aeronautics and Astronautics

Acknowledgments

This project was sponsored by the CC++ Group at the MIT Media Lab. I wish to thank the people of this group, Betty Lou McClanahan, Ryan Chin, Melissa Potter, Jim Meyers and others, with whom I shared great moments such as visits and presentations to the sponsors of the group.

I am grateful to Professor Hall for his advising and rigor, especially during the editing of this thesis. Some truly helpful comments about applications of shape memory alloys and multidisciplinary system optimization also came from Professor De Weck, from the Department of Aeronautics and Astronautics at MIT.

My original lab in the Department of Aeronautics and Astronautics was the Active Material and Structures Lab. I truly appreciate the support and comments from the people there: Dr. Mauro J. Atalla who gave me my first opportunity to work within the lab, the students (Cyrus, Lodewyk, Song, Onnik, Tim and Kris) and personnel, Mai Nguyen, Dave Robertson and Marie C. Jones.

My last word is for my other friends from all over the World who I expect to meet again all over the World as well. And Anne.

Contents

List of Figures

List of Tables

Chapter 1

Introduction

1.1 Background

The aerodynamics of a sports car has a large influence on its performance as well as the design of some parts of the car, such as the suspension system [5]. In particular, some sports car designs use extractors – or Venturi tunnels – under the body of the vehicle to provide downforce to increase its traction, which improves maneuvering performance. This design is motivated by the low amount of drag created by Venturi tunnels, compared to other options, such as wings and spoilers. However, a major drawback of using Venturi tunnels is that the amount of downforce produced increases with speed, causing the body of the car to pitch. The shape of the extractors can be optimized to provide a given amount of downforce with the lowest possible amount of drag, as shown in [6]. However, the optimization cannot remove the issue of the pitch angle, so that complex solutions have to be developed, in particular for the design of the suspension system, to prevent this undesirable effect.

An alternative idea for the design of sports car using Venturi tunnels is to have the shape of those tunnels vary with the speed of the car. By doing so, the amount of downforce produced can be tuned so as to reduce their intensity at high speed, and, as a result, prevent the pitch to degrade the performance of the car. As shown in Fig. 1-1, the Venturi tunnel should become less efficient at high speed, that is, it should be less open so as to provide a smaller lift coefficient, so that the absolute level of downforce does not increase unduly with speed. In order to provide actuation to the structure, active materials seem to be a suitable solution.

1.2 Active Material Selection

Active materials are a class of materials that can be deformed upon the application of a control signal, which may be good alternatives to traditional actuators such as pumps and motors for some shape-deformation applications. Indeed, they are more

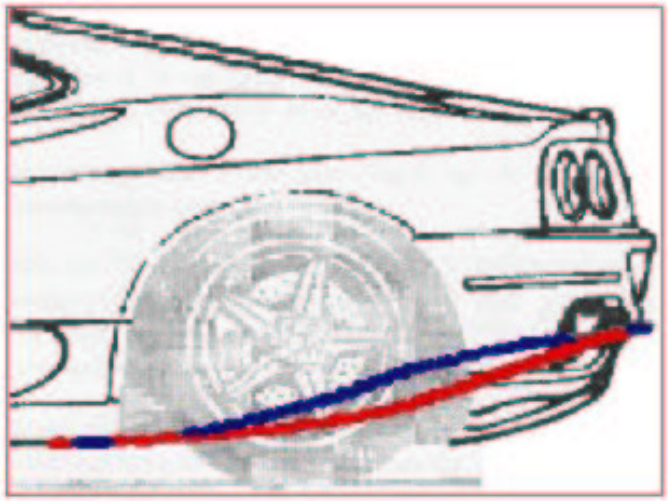

Figure 1-1: Variation of the shape of the extractors, profile view. The blue profile corresponds to the low-speed, high efficiency configuration. The red one is the less efficient shape at high speed.

space-efficient, and can lead to low-weight actuation systems. A benefit they also offer is a simplification of the actuation system, as they can be embedded into structures.

A broad overview of the field of active materials is available in [1]. It is possible to split active materials in different categories with respect to the actuation principle that is involved to drive them. Most active materials are activated by one of three types of fields:

- **Electrical fields**. Electrostrictive and piezoelectric ceramics and polymers (PZT, PZNPT, etc.) are driven by a voltage applied to the samples, and/or can provide a voltage when they are deformed.
- **Magnetic fields**. Magnetostrictive materials, magnetic shape memory alloys are driven by a magnetic field, which allows for contactless actuation. However, they have the major drawback of requiring sometimes massive coils to perform the control.
- **Thermal fields**. Shape memory alloys are actuated by a change in temperature. Nitinol, a compound of nickel and titanium plus minority species, is the most widespread of such alloys. Heating is often achieved by Joule (resistive) heating, that is, by passing an electric current through the wires. Cooling is a more subtle issue that will be addressed later in this thesis.

We can compare the different performances of active materials. Such a study can be found in [4], which is summarized in Table 1.1. This table gives a feeling of what the characteristics of the different actuation systems are, and how they compare. We notice that SMAs are by far the most suitable active material to provide work, even compared to traditional systems. Such alloys are indeed known for their ability to

Table 1.1: Comparisons of significant values among active materials and traditional actuation systems, from [4].

	Stress (MPa)	Strain (%)	Efficiency (%)	Bandwidth (Hz)	Work (J/cm^3)	Power (W/cm^3)
Piezoceramic	35	0.2	50	5000	0.035	175
Single crystal piezoelectric	300	1.7	90	5800	2.55	15000
SMA	200	10	3	3	10	30
Human muscle	0.35	20	30	10	0.035	0.35
Hydraulic	20	50	80	4	5	20
Pneumatic	0.7	50	90	20	0.175	3.5

provide large strain and stress. Thus, when the actuation needs to provide significant dispacements and forces, but with no major requirement in term of the time response, SMAs figure as the best choice to make. In the present project, this has led us to choose them, Nitinol in particular. It was expected that they would simplify the design of the actuation system by requiring less amplification. In addition, the actuation time was overlooked as a constraint because of the low speed requirement of the application. Other sources support the conclusions drawn from this table and provide more insight on the different active materials. See for instance [1], from which the chart comparing the density of work available is presented in Fig. 1-2. This chart emphasizes again the benefits expected from SMAs with regards to other active materials: for the same work output, much less mass of material is required to perform the actuation. Only hydraulic systems are expected to be better with respect to this metric. However, the use of pumps, tubes, etc., is expected to complicate the implementation of hydraulic systems as compared to SMAs.

An important point appears from Table 1.1. Active materials each have their benefits and drawbacks. For instance, SMAs are able to provide much more work, yet they can not be actuated at high frequency. So, they can only be expected to provide little power, compared to piezoelectric ceramics. Therefore, the field of active materials would benefit from material research (and characterization efforts) in order to search for better performing materials. Such a higher performance material is presented here, the single crystal piezoelectric – although the cost of such a material is likely to be high. Another issue to account for in the selection of the actuation technology is its maturity. Active materials have not been widely adopted in commercial applications, due to their relatively low technical maturity.

As a result of such comparisons, shape memory alloys were selected to perform the required actuation. Issues related to this choice are the main points addressed in this thesis, and arguably its main contribution. Indeed, the application of SMAs to actuator design has been somewhat left aside compared to the numerous efforts on piezoelectric actuators. This thesis seeks to propose a complete methodology for

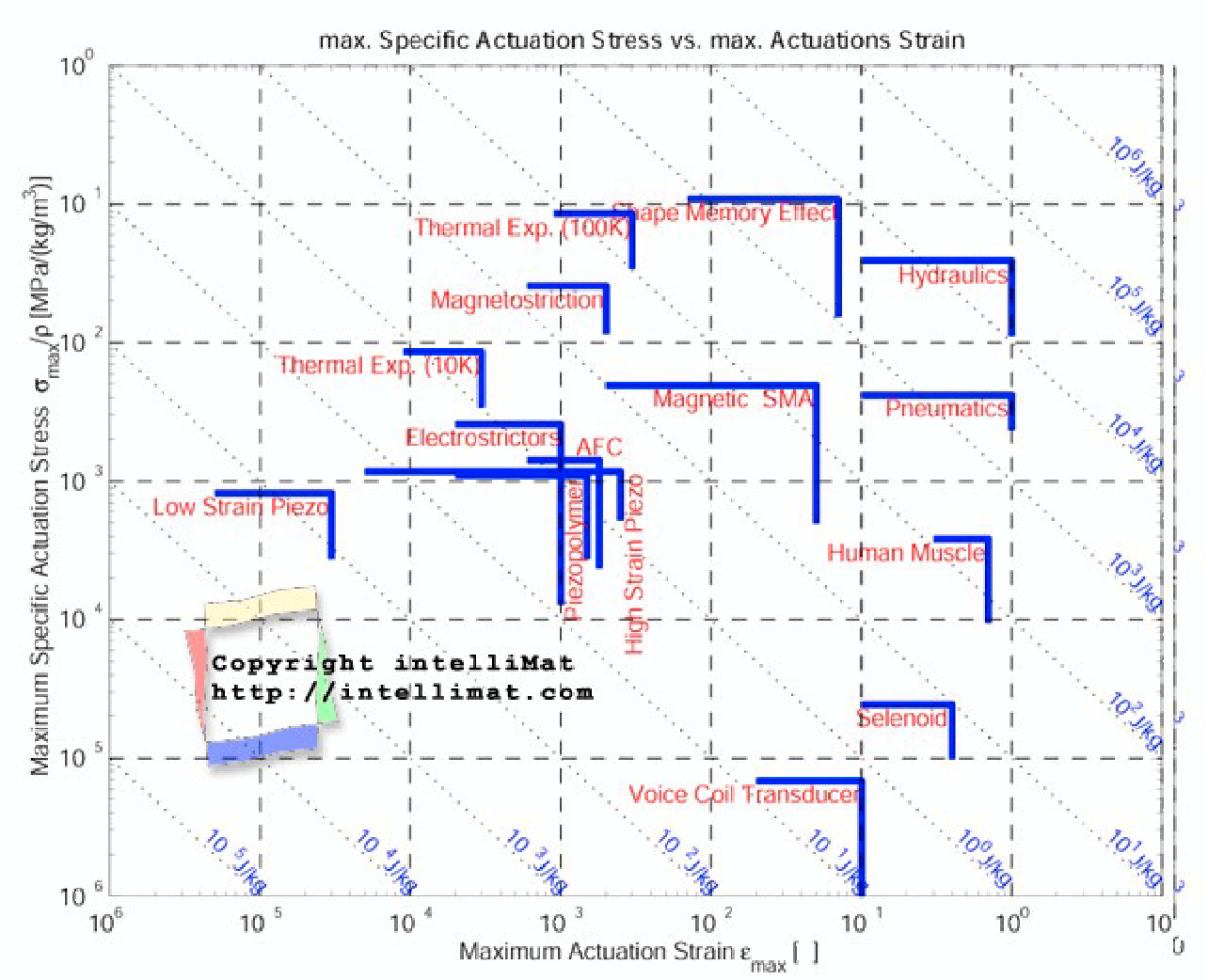

Figure 1-2: Stress-strain product chart for active materials, from [1]

designing with SMAs, and also includes a discussion on the performance metrics to use with such materials. Then, the topic of Chapter 4 is to look at trade-off issues raised during the implementation of SMAs to the development of actuators.

After choosing to use SMAs as the active material, we should select what kind of alloy to consider. The properties of SMAs depend on and are very sensitive to the concentration of the different compounds inside the alloy. No thorough discussion is available on that subject, yet many references do consider such variations [7]. Hence the most common practice is to consider only a limited set of compounds, thus limiting the variety of performances offered. In Reference [8], we can find a comparison between Nitinol (NiTi), which is by far the most common SMA, and CuZnAl and CuAlNi. Some major characteristics are presented in performance charts, in a way that can be compared to selection charts for engineering materials [9]. With respect to such metrics as output volumetric work per unit of mass, resistive heating capability,

characteristics variation with cycling, NiTi is identified as the most suitable of those shape memory alloys, while there is only a slight difference in cost. While this paper does support the choice of using Nitinol compared to other varieties of SMAs, we should advise that a careful check be performed with the samples to be used in the application. This caution is suggested by the fact that all the plots provided there show large variations of the properties. More generally, there is no database available on shape memory alloys that could make it easier to choose an alloy that would be the most suitable for a specific application.

1.3 Shape Memory Alloys Devices

SMA actuators fall into two main categories. The first uses the one-way behavior, while the second makes use of the two-way to produce cycles. The two categories have not developed in parallel; the former is by far the most developed one, while the latter can be seen as a research topic. We illustrate this difference of maturity through past or recent applications. In addition, we include a survey of applications in which SMAs feature unique benefits. Passive applications are cases in which the sensing and actuating capabilities of such materials are used without additional control mechanism.

1.3.1 Applications of One-Way Shape Recovery

One-way shape recovery is a process where once the actuation takes place, the material will not be expected to deform again. A successful application of one-way recovery has been the Cryocon© connector by Raychem Corp. The Cryocon is a connector used for joining tubes, in particular for aerospace systems. It takes the form of a ring of SMA, the transition temperatures of which are set very low. The ring is stretched at very low temperature (in liquid nitrogen), and passed around the tubes to be connected. Once the nitrogen is removed, the ring squeezes the tubes, thus connecting them. The connectors have the benefit of being cheap and strong. Most of all, they do not necessitate high temperature treatments such as welding that could damage the tubes. In addition, they are corrosion resistant.

Other applications of this behavior have been developed. For instance, the capability to detect a temperature rise has been used for valve control systems, fire-safety (sprinklers), or heat control device. This variety of products has made SMAs the most widely used active material at present.

1.3.2 Applications of the Two-Way Behavior

Applications using two-way behavior are based on a reversible shape recovery. Many potential applications of the two-way behavior have appeared in the robotic community. SMAs are primarily considered as capable providing a large energy output.

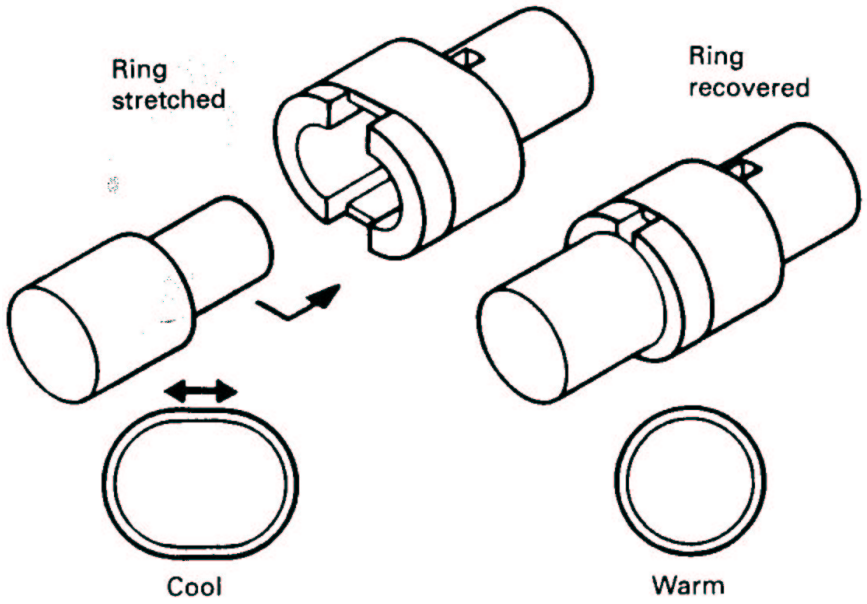

Figure 1-3: Cryocon© connector, from Raychem Corp.

Furthermore, they can be easily embedded. For example, resistive heating is used for heating, thus they do not necessitate pumps or other additional devices. These characteristics have led for example to the development of artificial muscles in the field of robotics. Those so-called muscles are in most applications merely wires used to actuate joints. They are mostly used with no consideration of efficiency. Last, most of the applications have been confronted with the issues of the actuation time and temperature control. An illustration of such difficulties can be extracted from the underwater biomimetic vehicle project [10]. This project attempted to develop a fish-like vehicle. SMA wires are used in an antagonistic way to produce the movement, with a target frequency of the order of $f = 1$ Hz. However, the still-air experimental results show an actuation time in the order of $t = 150$ s. Furthermore, the immersion of the vehicle in water would certainly improve the cooling of the wires, thus reducing the actuation time. However, by maintaining the device in a very large heat sink, the heat losses will be such that it is estimated the actuation power will be increased by a factor 20. Clearly, SMA users should be aware of such constraints in the development of applications.

Other works do not address the time issue, as the applications considered do not necessitate fast response. This is the case of a helicopter rotor blades tracking device presented in [11]. In that project, the prime benefit expected from SMAs is their large stroke. Grant and Hayward [12] have developed large strain SMA actuators for the articulation of robotic cameras. They use a nonlinear setup to provide large displacements. The design process does not consider the issue of the force required; the amount of force is just presented as a by-product. This issue is thus not addressed in a very systematic way. In addition, the SMA samples used in the work are chosen very thin (100 μm diameter wires), which results in quite good actuation times. But

again, this is not designed for *a priori*.proposed for the actuator is quite complex.

At a different scale than the one of interest in this thesis, the high energy density of SMAs has lead to a significant push to use them for MEMS (Micro ElectroMechanical systems). For instance, [13] presents the development of a micro-pump using SMAs. The main characteristic of the pump is a high pressure differential. The capability to handle large pressure differentials is mainly a benefit provided by SMAs specifically, instead of any other active material. In addition, at MEMS scales, the utilization of SMAs makes the issue of thermal control easier. Indeed, much less energy levels are handled by the wires. In addition, at those scales, device such as thermoelectric Peltier coolers can be used.

We can also include in this review the intensive research undertaken to develop models to capture the shape memory effect. Those works will be discussed in subsequent chapters of the thesis, while an example is detailed in Appendix A. Those models are not very useful for actuator design, as their complexity makes them suitable for *a posteriori* dimensioning only. Some simple rules of thumbs have been proposed to develop bias spring actuators, as in Waram [14] and Duerig [7]. However, they do not estimate such key quantities as the actuation time.

1.3.3 Other Applications of SMAs

There exist additional potential utilizations of the shape memory effect that are not related to the present work. We present different ideas that have been pursued that exploit the benefits offered by SMAs. The first idea is based on the fact that the shape memory effect can be described as a variation of the stiffness of the material. This variation can be used for frequency tuning of systems. The possibility of using this characteristic to prevent the thermal buckling of the panels on supersonic aircraft has also been investigated. Indeed, embedding SMA wires into the panels could make the stiffness of those increase at the high temperatures occurring at supersonic fight regimes.

We should also mention a distinct behavior featured by SMAs when used in certain conditions (Duerig [7]). This behavior is called superelasticity. It is a spontaneous recovery of the shape at ambient temperature. Thereby, a sample that is plastically deformed would recover its shape without any temperature change. This phenomenon is close to an elastic behavior, although the material does sustain plastic deformations. We should underscore that SMAs are metallic compounds, thus they have such characteristics as a large stiffness and good conductivity. Superelasticity has thus been used primarily for cell phone antennas. In mechanical engineering, this behavior could also be used for its high energy absorption capability. Thus, superelastic elements have been envisioned for applications as passive damping systems.

1.4 Overview of the Thesis

The task addressed in this thesis is to design an actuator to povide actuation for the deformation of a car undertray. We need to overcome implementation issues such as those mentioned above. Therefore, we will emphasize the importance of incorporating all measures of performance in our model in order to avoid any contradictions at the stage of the implementation of the device. As a result of following this process, we will reach the conclusion that SMA actuators are not suitable for the sports car application envisioned here. Nonetheless, we will exploit the understanding offered by our model to emphasize the critical points that could make such actuators a viable option.

In Chapter 2, the shape memory behavior is explained, keeping in mind the application to actuator design. Then, a first model is developed for a generic SMA actuator. Next, in Chapter 3, different design options are presented and discussed. The question of differentiating them leads to the definition of a set of possible design performance metrics, as well as the design variables and constraints. In Chapter 4, an actuator setup is selected and modeled. Subsequently, a thorough design space exploration is achieved and discussed, leading to the identification of the best practice in term of SMA actuator design. Finally, Chapter 5 concludes the thesis, with a summary of the results, and recommendations for future research.

Chapter 2

Models of Shape Memory Alloys

In this chapter, we present the basics of the shape memory behavior. The details of the models drawn from the literature can be found in Appendix A as they are not the focus of this work. Rather, selected models of the shape memory effect are used to build a new model for shape memory actuators. This full model of the actuators features a simplified method to determine the amount of energy provided by the shape memory alloy. Using this approach, the amount of shape memory alloy required for a given application can be estimated. In addition, we incorporate specific characteristics of the shape memory effect in the model. Those characteristics will have us modify the original set of requirements.

2.1 Principles of Shape Memory Behavior

The shape memory effect (SME) is due to a reversible thermoelastic phase transformation. Materials exhibiting this effect have two stable phases, one at high temperature called austenite, and the one at low temperature, the martensite phase. Varying the temperature of material samples results in the transition between the corresponding two crystalline configurations.

The concept of memory resides in the fact that upon heating, such a material is capable of transitioning from the martensite to the austenite configurations Fig. 2-1. The sample hence undergoes possibly significant deformations when it turns into the austenite configuration, as if this was a shape it had the memory of. This effect is mainly used in the following way. First, the sample is annealed at high temperature (usually over a period of time), with a certain shape imparted. Then, it is cooled down to a characteristic temperature (under which there is only the martensite phase within the sample) and deformed to take the non-actuated shape. Finally, upon heating, the sample will recover at least partly the previous high temperature shape. A version of this procedure is used for SMA wires. Instead of being annealed at high temperature, the wires are plastically stretched in the martensite phase. Then, upon heating, part of this pre-strain imparted to the wires is recovered. This process is

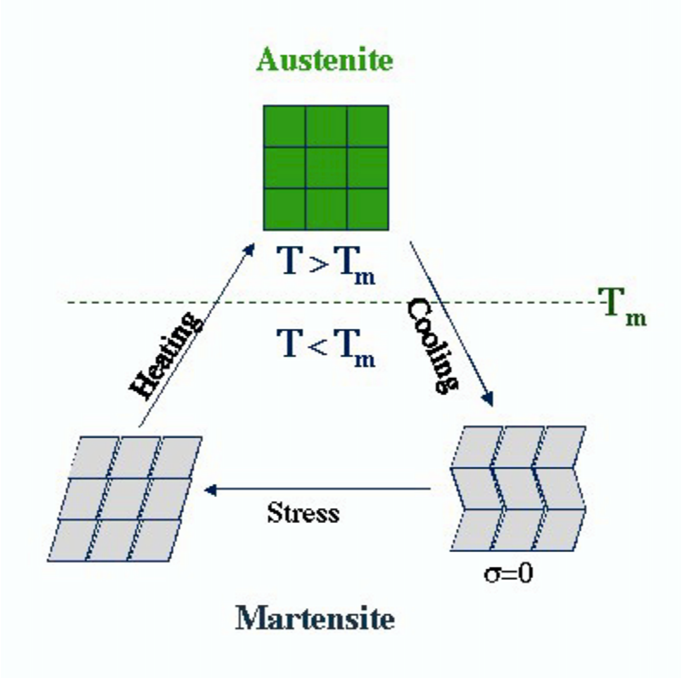

Figure 2-1: Phase transitions taking place in the shape memory effect [2].

exactly the same mechanism as previously presented – the length of the wires before stretching is equivalent to the annealed shape.

With the shape memory effect as described above, the material will not return to the original austenite shape when cooled. Indeed, once the shape is recovered on heating, the sample remains in this configuration. On the other hand, many applications require cycling between the low- and high-temperature phases, in order to produce a cyclic motion. There are different ways to achieve cycling SMAs. It is possible to train the samples to exhibit this two-way effect. Under no load, it is then possible to switch back and forth between the two configurations. However, this trained behavior is known for not being stable upon cycling, and eventually the memory fades away (Duerig [7], Otsuka [15]). A more effective way to produce a two-way effect is to create it artificially by using a bias that stores the energy produced by the SMA material, and is capable of restoring the shape when the sample is cooled down. This bias may be a constant force (a mass for instance, as in Fig. 2-2) or a passive spring. Alternatively, one can think of using another active SMA sample as a bias, thus producing an antagonistic actuator as presented in [16]. One sample is actuated, producing deformations in one direction, then it is cooled while the antagonistic sample is heated. However, many issues are raised by this kind of configuration, in particular the non obvious interaction between the phase transformations in the two sets of SMA. Indeed, when switching the actuation from one set to the other, some residual heat remains that makes the next actuated set work against still active material. This fact is a limiting factor for antagonistic actuator configurations. Furthermore, this option is found not to be efficient from the perspective of heat transfer.

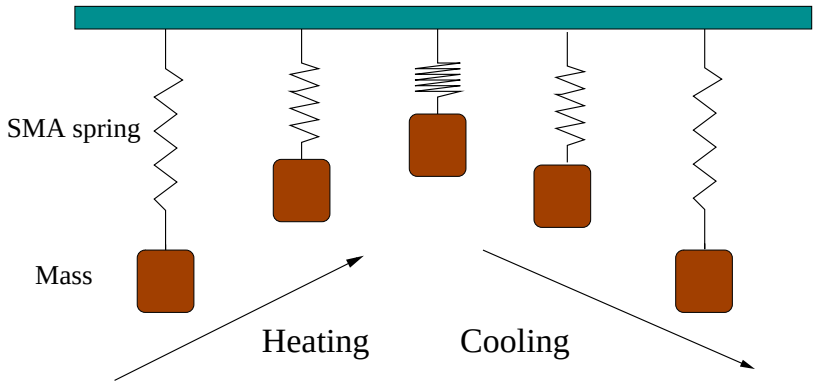

Figure 2-2: Illustration of the two-way shape memory effect. Mass used to produce the bias load, adapted from Hodgson [3].

Shahin *et al.* [17] provide an analysis of the efficiency of antagonistic setups.

Transitions taking place during the SME are characterized by start and finish temperatures. These temperatures are denoted in Fig. 2-3 by A_s and A_f respectively for the austenite phase, and M_s and M_f for the martensite phase. Those transition temperatures are in fact stress-dependant – they increase linearly with the applied stress (see Appendix A).It should be noted that the two-way effect is characterized by a significant amount of hysteresis. Indeed, the transition temperatures do not coincide between the austenite to martensite and reverse paths. The amount of this hysteresis varies according to the kind of alloy used. For the most common one, used in this thesis, the difference is about $\Delta T \approx 30$ C.

Importantly, both the one-way and two-way shape memory effects have potential applications (see Duerig [7] for example). However, in the present thesis, the two-way behavior is required. Furthermore, the issues cited above lead us to use the passive bias solution to produce the two-way effect.

2.1.1 Mechanical Modeling of SME

Numerous one-dimensional mechanical models for the SME are available. The most relevant ones are discussed here. Those models generally have two distinct parts. One is the constitutive relation, that links stress, strains and temperature. In substance, constitutive relations are based on energy considerations. The constitutive relation given by Tanaka [18] is

$$\dot{\sigma} = E\dot{\epsilon} + \alpha\dot{T} + \Omega\dot{\xi} \tag{2.1}$$

In this expression, σ is the stress in the sample, ϵ the strain and E the Young modulus, T the temperature and α the thermoelastic expansion coefficient, and ξ is the phase fraction of the martensite phase, with Ω a coefficient that accounts for the effects of subsequent volume changes on stress. The time derivatives indicate that this relation really holds for variations of those variables. This formula is a basis for many other

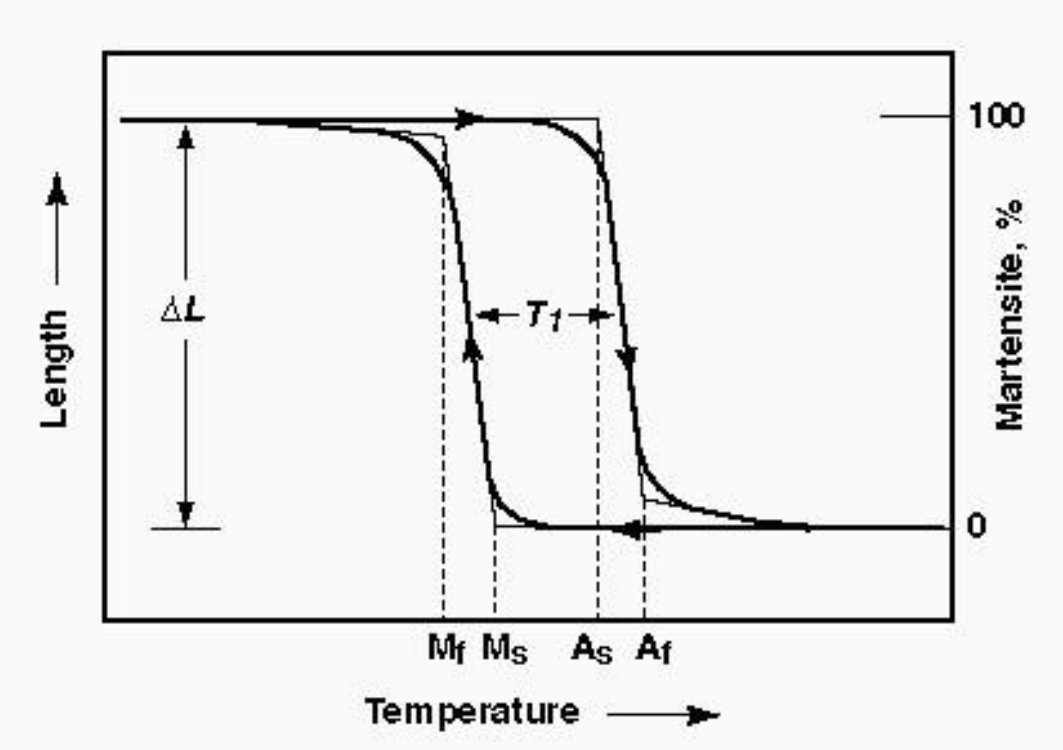

Figure 2-3: Typical transition curve for SME, featuring the hysteresis, from Hodgson [3].

models. The equation features the coupling between temperature, strain and induced stress. It is obviously linear.

The second part of the proposed models for the SME is the kinetic law that captures the evolution of the transformation (phase fractions). In order to close the model, the kinetic law is derived or, more often than not, given *a priori* as

$$\xi = \text{function}(T, \sigma) \tag{2.2}$$

Some instances of the expression of this function are provided in Appendix A. These functions are chosen to feature the same behavior as in Fig. 2-3. They are often described by parts, according to the direction of the transformation and the phase in which the material is. Therefore, the resolution of the equation of the SME involves a rigorous tracking of the transformation and the phase fractions. Bekket and Brinson [19] provide a complete discussion about the different possible phase transitions. In addition, Lagoudas *et al.* [20], [21] have derived a so-called return mapping algorithm that is not based on an explicit formula for the phase fraction. However, it still highly couples all the states in the computation: temperature, phase fraction and stress.

Some details of the models of SME are presented in Appendix A. However, Brinson and Huang [22] note that most of the models propose equivalent constitutive laws. The differences in the kinetic laws affect the accuracy of the results or capture

differences in the SME in different alloys, such as the transition temperatures or the width of the hysteresis.

2.1.2 Thermal Models

The shape memory has been presented as thermally induced, hence the thermal modeling of the problem is of prime importance. At stake here is the identification of the transfer function between the control signal, understood as being the process that creates the temperature change in the samples, and the induced transformations. Two models that attempt to answer this question are sketched here, and described in greater details in Appendix A. The first of those models is a heuristic curve-fit from a number of experiments, due to Waram [14]. This model relies heavily on experimental coefficients. However, it is able to capture the relationship between the input current used in heating SMA wires through resistive (Joule) heating, and the time to heat and cool down the wires. The important parameters are the transition temperatures for the shape memory effect (which are stress-dependant), and the environment through the ambient temperature and convection coefficient. From this formulation, the input current must be large enough to allow full transitions (*i.e.* enough heating) to take place.

The second model for the thermal problem in SME is an adaptation of the heat equation, presented by Lagoudas [23] (see Appendix A). The model provides a law for the heat capacity of the SMA. Otherwise, it is based on essentially the same parameters as the previous model. Yet, the formulation as a differential equation raises the issue of having to actually solve this equation (for a given input current law) before having access to actuation time. Thus, this model requires significant computational efforts, whereas the previous one rather provides formulas to estimate directly the transition times.

However, in most cases, researchers working on SMAs have been mostly interested in predicting the behavior of a system when the temperature history is prescribed. This prediction problem is only relevant if the temperature is effectively available, from the signals from thermocouples for instance. Although adding thermocouples may be feasible, we really need to incorporate the model of the process that provides the energy to the samples in order to size the actuators *a priori*, and in particular to predict the actuation time of a given system.

2.2 Models for Shape Memory Actuators

In the task of designing actuators based on active material, it is important to use models of the behavior of those materials that capture the phenomenon with sufficient accuracy. More importantly, those models should be tractable enough to be embedded into the design process. Most of the mathematical models introduced above do not satisfy this condition – they do not provide useful quantities directly, such as the

energy provided by the active material. This section thus presents more suitable models of SME. We introduce assumptions to assess the stress and strain produced during shape recovery. We will apply them to a theoretical actuator setup at the end of the chapter, to determine the volume of active material required in the present case.

2.2.1 Amount of Energy Provided by SMA Samples

We restrict the discussion here to one-dimensional SMA samples, *i.e.* wires. SMAs are most widely used in this form. From Liang and Rogers [24], a graphic helps determining the relation between the characteristics of the SMA, the pre-strain initially imparted to the sample, and the energy that is provided. This graphic is built from a piecewise linear description of the stress-strain characteristic of the two phases of SMA. Then, it is assumed that the heating process makes the operating point going from the martensite line to the austenite one, according to a path that is set by the stiffness of the load against which the recovery process takes place. Fig. 2-4 illustrates those characteristics. Here, we consider mainly linear loading conditions, while Chapter 3 will include a discussion on what are the effects of using a nonlinear load. As a result, an expression of the energy E provided by the SMA sample is

$$E = \frac{1}{2} F d \tag{2.3}$$

where F is the recovery force, d the corresponding displacements, the expression of which can be derived from graphs such as Fig. 2-4 as a function of the mechanical coefficients corresponding to the two phases of the alloys. An alternative description is the energy density e of the material, expressed as

$$e = \frac{1}{2} \sigma \epsilon \tag{2.4}$$

in which σ is the recovery stress and ϵ the associated strain. Importantly, the volume of SMA required for actuation is

$$V = \frac{E}{e} \tag{2.5}$$

Hence, from the characteristics of the phases of the SMA, we can estimate the volume of active material required to provide the necessary amount of energy to deform the structure.

2.2.2 Details of the Model for Energy Estimation

We need to emphasize some details of this model. In the first place, it does not deal with phase fractions as one would expect, as phase fractions are important variables during the shape memory effect. However, this issue is blended into the path taken by the transitioning SMA sample, which necessarily follows the load characteristic.

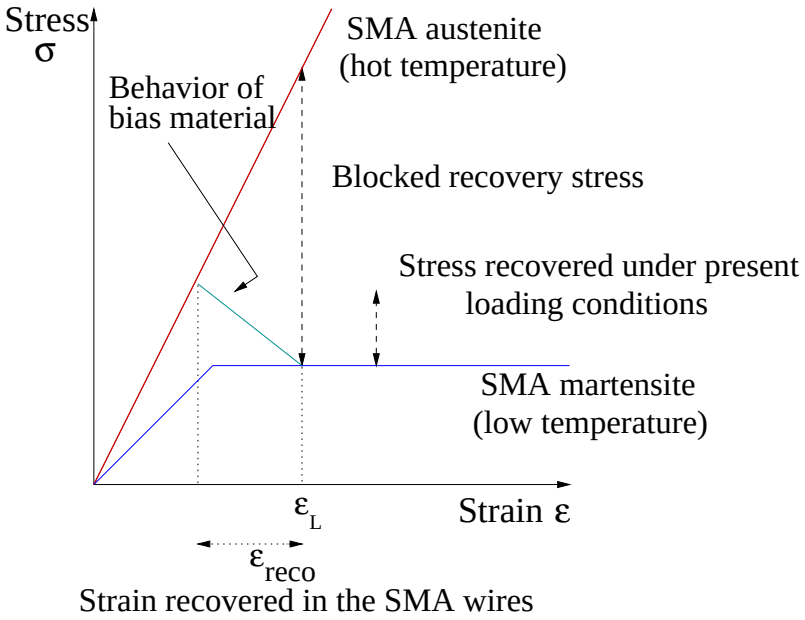

Figure 2-4: Characteristic of martensite and austeniste phase. SME transition against a linear load.

It is necessary to ensure that full transformation takes place at each cycle, otherwise the high- and low-temperature characteristics must be changed to account for the evolution of the phases within the material.

Also, in the graphs, we introduce the concept of stiffness as seen from the SMA wires. This stiffness describes the displacements at the location of the wires for a given force applied on the load. It is the actual stiffness of the load extended to include the effect of amplification of the displacements between the location of this load and the location of the wires. In particular, this concept of stiffness corresponding to the displacements of the SMA wires makes us handle a linear stiffness even though the load may in effect be a rotary spring for instance (see Chapter 3, the illustrative configuration). In effect, the load stiffness will come from both external operating conditions (aerodynamic loading) and an internal stiffness within the actuator itself.

2.2.3 Other Models for SMA Actuators

As mentioned before, we will use explicit heuristic formulas to estimate the heating and cooling times. These formulas follow from very simple models for the current and electric problems. On the other hand, they rely on the estimation of the transition temperatures, which is a more advanced topic. The transition temperatures are stress dependant. Therefore, the thermal model of SMA actuators should capture this dependency. The estimation of stress is derived from impedance matching considerations, which will be introduced more formally in the following chapter. We use a reverse engineering procedure to go from the loads within the actuator back to the stress into the wires. The external and internal problems, respectively the estimation

of the loads provided by the actuator and those residing in the SMA wires, have to be linked. They are indeed connected through the concept of impedance matching. From the knowledge of the loads on the actuated structure (specifications) and the value for the impedance matching performance of the device, we can find the stress in the SMA wires, thus estimate the transition temperatures. Appendix B presents the whole process.

In addition, we will need to deal with an issue of actuator placement. In the case of actuation using a device located along the span of the structure to be deformed, we propose a rough estimation of the placement. This method uses energy considerations in order to compute the total stiffness of the device when placed along the structure. Then, some assumptions on the relative stiffness between the different actuators used allows us to find a location which meets the requirements. Our approach to solve the actuator placement issue is again presented at the end of Appendix B.

2.3 Presentation of Requirements and Consequences on Specifications

The requirements on the design of the actuation system originate from the desired task, namely deforming a Venturi tunnel. The requirements include constraints related to the environment and operating conditions, in the context of sports car design.

Required force and displacement. The displacements are set to provide a shape change relevant from an aerodynamic point of view. The maximum displacements are set to $\Delta l = 3$ cm, understood as the displacements of the surface at the middle location. A variations of the downforce of $\Delta F = 200$ N sets the stiffness required for the actuation system, which must counteract this variation of force.

Actuation time. It is required that the transition from non-actuated to full actuated shapes and back takes place within $\Delta t = 3$ s.

Power. The power requirements are limited by the power available. A maximum power of $P = 2000$ W can be used over a short time. The operating voltage is typical for automotive equipment systems ($V = 42$ V).

Number of cycles. The system must be able to work over a sufficient period of time, translated into a number of actuation cycles. In the present case, this number is $N = 50000$ cycles. This requirement is translated into a maximum recovery strain that can be achieved over this amount of cycles. This requirement limits this strain to $\epsilon = 2\%$ (see [25]).

Added mass. Heavy mechanisms cannot be viable. For the current application, the maximum allowable mass of the actuation system is $M = 20$ kg/m^2 (mass per unit of surface covered by the deformable structure).

Ambient temperature. The temperatures at the location of the system are in the range $T = -40$ C to 125 C. This operational temperature range may interact with the transition temperatures characterizing the shape memory effect.

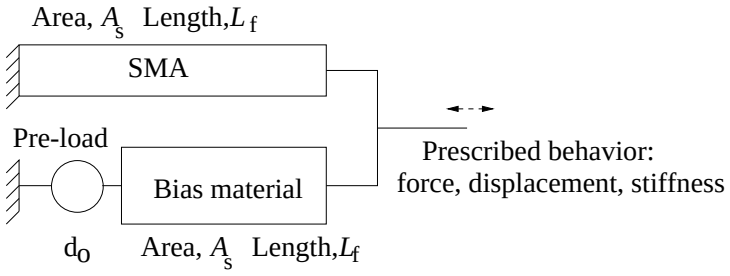

Figure 2-5: Generic actuator schematic.

2.4 Theoretical Actuator Setup, Preliminary Check for Feasibility

The setup illustrated in Fig. 2-5 is a generic actuator that allows us to capture the behavior of generic SMA actuators. It is composed of a SMA sample, connected in parallel with a load that is represented by an offset (pre-load) and a stiffness.

A consequence of this generic setup is the identification of further design restrictions that apply on SMA actuators. In particular, some pre-strain must be present in the actuator in order to produce cycles. This pre-strain is achieved by inserting a mechanism that is capable of stretching the wires back to a plastic-state martenstite phase after a heating phase. However, we realize by sketching the full characteristic of the actuator in the non-actuated state Fig. 2-6 that the device is soft in the low temperature state. This relative softness may result in unexpected further deformations of the SMA sample in the cool state. Those deformations would in turn change the behavior of the actuator. In order to avoid such unexpected variations of the performance of the actuator, we should embed stiffness into the device itself, so as to provide sufficient stiffness even without actuation in order to prevent the martensite phase from varying unexpectedly.

Remark on the choice of bias material. The choice of material for the bias mechanism is guided by the need to minimize its volume or its mass, and should account for the possible interaction with the active material (*e.g.*, the material should not melt under the heat provided to actuate the SMA sample). We selected steel for this task of providing stiffness to the actuator. Indeed, the selection is based on the same idea as spring material selection. We can find in Ashby [9] that steel does figure among the best materials for such a purpose. Additional characteristics, such as good thermal stability and lack of creep (compared to rubber, another good alternative material for springs) add justification to this choice.

Another decision to make about the bias mechanism is its configuration. We choose to use a leaf spring in order to make it possible for the bias to absorb the large deformations of the system.

Estimation of the volume of SMA required. With the models presented above for the energy available from the SMA samples, also with the theoretical setup shown in Fig. 2-5, we are able to estimate the volume of SMA required. As for the

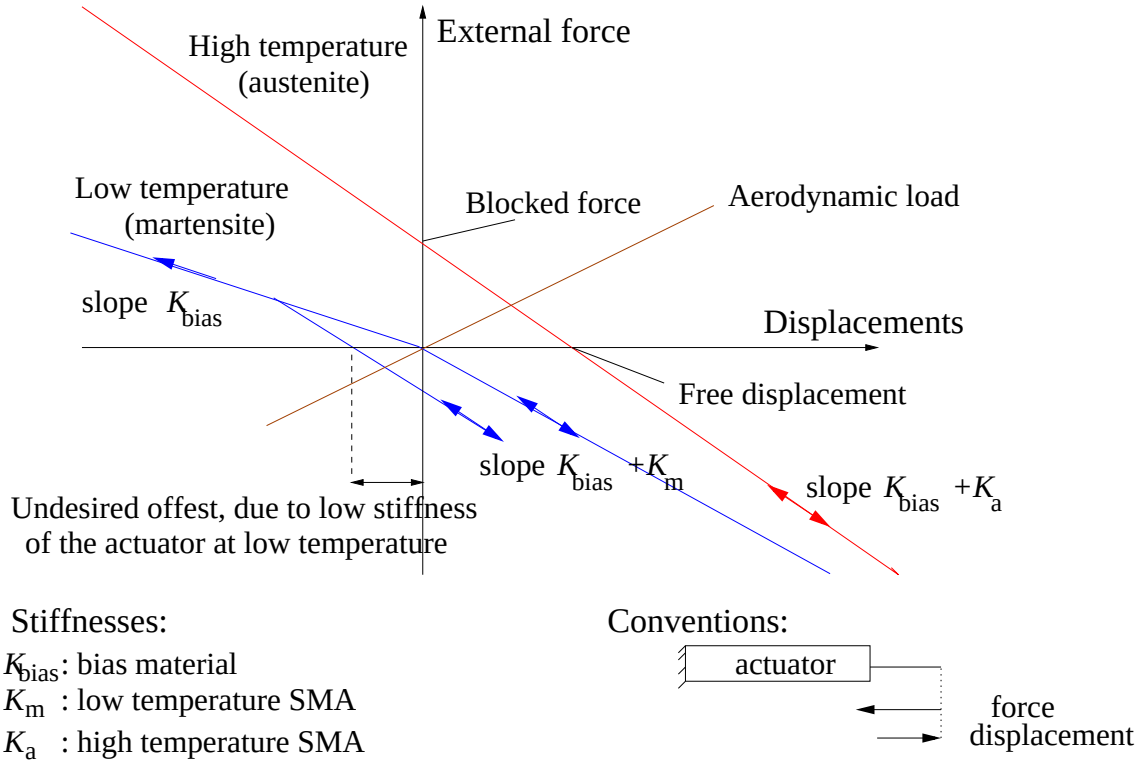

Figure 2-6: Full characteristic of the actuator, in actuated and non actuated conditions. From those conditions, we identify the risk of having a soft cold characteristic that can yield changes of the actuation performance of the actuator.

bias, the efficiency of leaf springs was taken from Ashby [9]. Furthermore, the amount of energy absorbed W was computed in a similar way as we have assessed the energy provided by the SMA sample, from

$$W = \frac{1}{2} F d = \frac{1}{2} \frac{(F_y)^2}{E} \tag{2.6}$$

where F_y is the yield force, E the Young modulus for the material considered.

Table 2.1 presents some results as applied to the specifications mentioned earlier. The amount of recovery strain ϵ in the SMA sample is varied. $\epsilon = 0.1\%$ represents a maximum value for piezoelectric materials as a matter of comparison, although such materials are heavier than SMAs and have comparable stiffness. $\epsilon = 2\%$ will be chosen in the rest of the thesis, while $\epsilon = 6\%$ is about the best value for shape memory.

These rough results show a great advantage in the utilization of SMAs, in terms of the energy they can provide. They confirm the choice of active material that was suggested in the first chapter of this thesis. These results also hint at the feasibility of the actuators, at least from a pure mechanical point of view – the mass requirements are not expected to be of concern. We note that there is a slight overlap between the ambient and transition temperatures. Thus, the environment could interact with the

Table 2.1: Estimation of required volume of SMA for the present problem, as well as the mass of the actuation system.

ϵ (%)	0.1	2	6
Volume SMA (m^3)	1.62×10^{-3}	4.04×10^{-6}	4.49×10^{-7}
Total Mass (kg)	10.8	0.287	0.286

actuators by switching them on unexpectedly. However, this issue was not considered to be critical. We could think of adding thermal isolation to prevent such interaction, ventillated during the cooling phase. In addition, the phase transformation is relatively slow at the beginning of the process, and reversible. So even if the transition is triggered unexpectedly by the outside temperature conditions, the effects in term of unwanted displacements of the structure would remain small. More importantly, this approach does not capture the specific utilization of SMAs, namely the heat transfer involved. The energy is estimated without accounting for the thermal process. In addition, it does not deal with any trade-off study, which would seek at optimizing the actuator design. This is the purpose of the following chapters.

2.5 Summary

In this chapter, we set the basis for the modeling of SMA actuators. From the mathematical models used so far in the literature to characterize the shape memory effect, we proposed more tractable ones that are suitable for actuator design. In addition, we used the specifics of the material in question to translate the requirements for the system into constraints at a material level. In particular, the amount of recovery strain achievable over the prescribed life of the device is limited. We also decided to include a stiffness mechanism within the actuator itself, in order to account for the relative softness of the non-actuated SMA sample. A preliminary result of this study is that the energy output of SMAs is sufficient for the current application. Therefore, we do not anticipate any issue from the mass requirement imposed on the device. However, the question of heat control and actuation time could be important issues.

Chapter 3

Design Methodology

In this chapter, we discuss several possible configurations for SMA actuators and the implications of those configurations on actuator performances. A simple strawman actuator design is presented. Although this particular setup was obtained heuristically, we can extract several design principles from the example that can be used to improve other designs. Specifically, design variables and constraints are identified, as well as the configurations that are expected to yield the most efficient actuators. The main contribution of this chapter is that it proposes guidelines for a methodology to design for some objectives. It brings in a sense of optimization of the device. On the contrary, most previous work on SMA actuators have focused on the *a posteriori* characterization of actuators. Here, the methodology rather relies heavily on capturing the interactions between the different phenomena involved in the shape memory effect at the preliminary stage of the design process.

3.1 SMA Actuator Example

In this section, an actuator setup is presented and its design pursued in order to illustrate a simple design methodology. The setup is based on heuristic ideas on how to meet the requirements in terms of stiffness and displacement.

The configuration of the actuator is composed of two arms linked with a circular portion, as shown in Fig. 3-1. The set of active wires is located on the external side of the ring section. The passive material of this section then acts as a rotary spring, whereas the arms transmit the displacements from the SMA wires. The useful displacements are then the displacements at the end of those arms. The idea behind this design is to get all the deformations at the same location in order to simplify the study of the stiffness of the device, and also the identification of the sources of compliance losses within the actuator. In the present configuration, deformations are located within the ring section. We expect the applied moment to remain fairly constant in this section, thus a circular ring of constant thickness is a suitable shape to bear those loads. The arms then provide the required amplification of the defor-

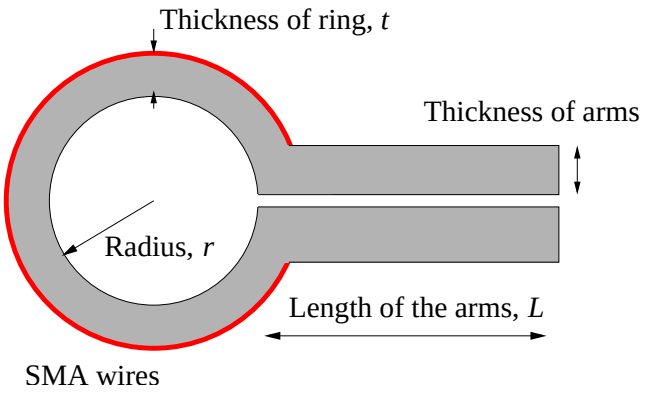

Figure 3-1: Setup of the example actuator. The SMA wires are located on the external side of the ring section

mations. It should be noticed that this design is similar to the piezoelectric C-block actuator concept (Brei and Moskalik [26]).

We address here the question of meeting the requirements with the proposed device. Those requirements are set in terms of stiffness at the end of the arms and required displacements. The analysis here is closely related to the one done previously for the theoretical actuator, with some adaptations regarding the specifics of the current setup.

3.1.1 Analysis of the Actuator

In order to fully design the device, several steps are taken. First, we analyze the factor that is expected to yield the most compliance within the device, namely the compliance of the arms. Thereafter, the stiffness of the rotary spring (ring section) is expressed as a function of the variables of the design. Then a verification of the proposed formula is performed using finite element modeling of the device. Last, the set of SMA wires used for actuation is sized in order to provide the right amount of energy.

Arm compliance. We can view the arms as being beams with one end free and the other one clamped through a rotary spring, as shown in Fig. 3-2. We are therefore interested in the equivalent stiffness of such a beam, being defined as the ratio of the force applied at the free end over the vertical displacement there.

By solving for the tip displacement in Fig. 3-2, we obtain the end stiffness K_{end} of the system from

$$K_{\text{end}} = \frac{F}{d} \tag{3.1}$$

$$\frac{1}{K_{\text{end}}} = \frac{L^3}{3EI} + \frac{L^2}{K} \tag{3.2}$$

Equation (3.1) is the definition of the end stiffness. Equation (3.2) is similar to the formula for two springs in series, as expected – the overall deflection is due to the

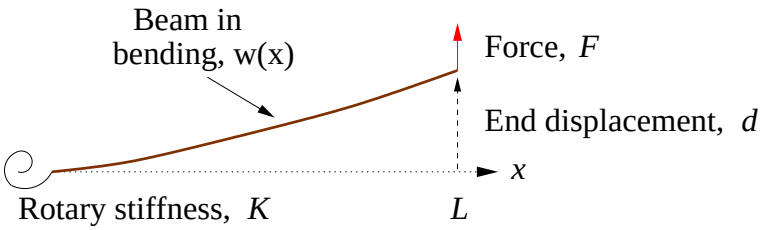

Figure 3-2: Schematic for the study of the beam compliance. One end is free, the other one attached through a rotary spring K.

rigid body rotation of the clamped end, and the bending of the beam. If we set K to go to infinity, we actually find the formula for the end stiffness of a beam, clamped at one end, free at the other one. Importantly, a coupling exists between the stiffness of the rotary spring and the bending stiffness of the beam. Thus, the two effects should be considered in the overall compliance of the system. However, we want most of the compliance to be into the bending of the ring part of the actuator, not in the arms, as mentioned in the previous section. Therefore, we have to compare the energy of the whole system and the energy in the rotary spring, which is done by defining *ad hoc* an efficiency η as

$$\eta = \frac{W_{\text{rot}}}{W_{\text{total}}} = \frac{\frac{1}{2}Kw'(0)^2}{\frac{1}{2}K_{\text{end}}w(L)^2} \tag{3.3}$$

The purpose here is then to make sure that most of the compliance is in the bending of the rotary spring, in order to minimizing undesirable compliance losses. Therefore the design should try to maximize this quantity η.

Rotary spring stiffness. The rotary spring, as used for instance in the discussion about the bending of the arms, is the circular ring section of the actuator. The angular stiffness of it is the ratio of the moment applied at the extremities of the open ring over the angle of aperture Θ. The end stiffness of the system must eventually be set to equal a value specified by the required empty stiffness of the device. The rotational stiffness K of the ring is estimated as

$$K = \frac{EI}{2\pi r} \tag{3.4}$$

where I is the bending moment of inertia of the ring section, and r its radius. Yet, the really useful quantity we are interested in is the end stiffness of the system, so we have to adapt equation (3.4). We get

$$K_{\text{end}} = \frac{K}{(L+r)^2} \tag{3.5}$$

Finite element analysis. In order to compare the formula and the actual value of the stiffness, a FEM model is used (Figs. 3-3, 3-4). By using FEM tools, we want to check the reliability of the model derived to characterize the actuator. The figures compare the stiffness at the end of the device as predicted by the formulas

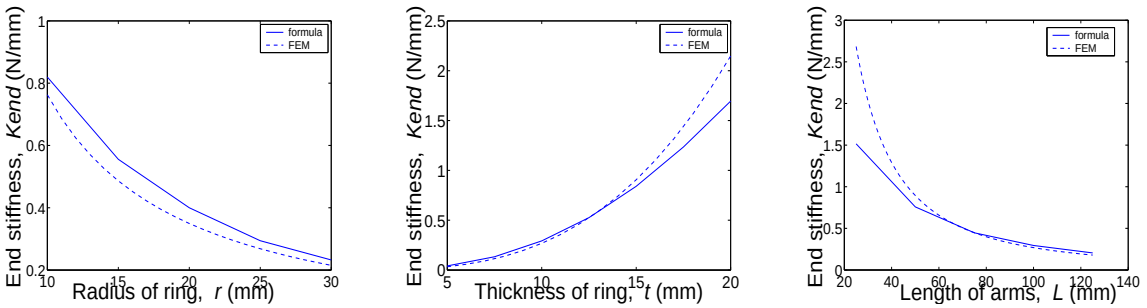

(a) (b) (c)

Figure 3-3: End stiffness as estimated from a FEM model, compared to the result given by formulas. Variations of (a) ring radius r (b) ring thickness t (c) length of the arms L, all other values fixed.

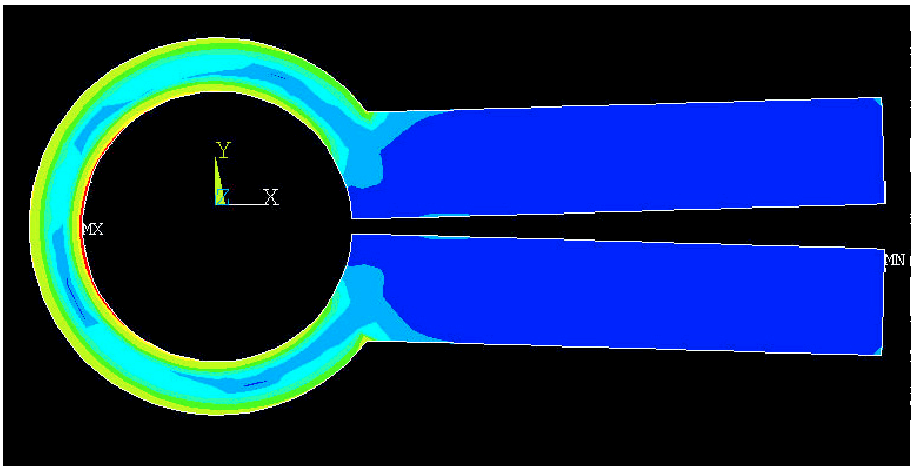

Figure 3-4: FEM model of the current actuator configuration. Strains in the deformed device. No bending occur in the arms, therefore we expect little compliance losses. In addition, the deformations are homogenous in the ring section such that the assumption of constant moment applied to this part of the device holds.

and using a FEM analysis as a reference. Different variables are varied. We can visualize the stress map within the device (Fig. 3-4), and look for violations of the assumptions, in particular the homogeneity of the stress in the ring section. Thus, some discrepancies appear, but can each time be directly related to some assumptions made to derive the formulas (*e.g.*, constant moment along the ring section of the device, deformations limited to this section only, etc). Yet, the magnitude and overall variation are preserved so that the formulas are relevant for a preliminary study of the device.

Sizing of the SMA wires. This step is intended to give the length and number (equivalently the stiffness and volume of the set) of SMA wires to provide the wanted actuation. The sizing is achieved using the same methodology as in the theoretical case with some modifications appropriate for the current configuration. In the previous chapter, a system composed of an active part and a bias material mounted in

parallel was designed in order to feature a given output stiffness and displacement. Here, the goal is to design the frame of the device according the requirement on the stiffness, then add the active wires. The stiffness as seen from the wires (K), which was introduced in Chapter 2, is expressed as a function of the specified stiffness at the tip of the device (K_{end}) as

$$K = K_{\text{end}} \frac{L + r}{r + t} \tag{3.6}$$

3.1.2 Design Trade-Offs

The purpose of the design process is summarized as followed. The system should bend mainly in its ring section. Therefore, the design should seek at maximizing the function η which is defined in the arm compliance study. Also, the actuator should have a given stiffness. This stiffness is estimated as shown above as a function of the required end stiffness. The length of the arms should be chosen such that we actually get the desired amplitude of the displacements between the tips of the device upon actuation. As the ring has to fit into the available space between the structure to deform and the upper wall, the radius of the ring section is constrained this way. There are additional constraints such as the maximum stress of the material in the ring section.

However, the constraints proposed here do not influence directly each design parameter or the performance of the system, such as its mass. This lack of correspondence is due to the setup chosen. For instance, the radius of the ring, its thickness, and also the length of the arms all play a role in the resulting output stiffness of the device. As a consequence, we adopt in the following section, the easy way to design the device. The maximum of variables are chosen *a priori*, then we compute the related ones so as to meet the requirements. Although this approach allows us to design the device, a more rigorous setup would be desirable that would make it possible to identify how each variable influences the design with regards to both constraints and performances.

3.1.3 Results for the Present Configuration and Comments

We present here the results obtained for the current configuration applied to the problem presented in Chapter 2 (Section 2.3). As mentioned earlier, we need to set some values arbitrarily and solve for the stiffness of the whole device. We take the ring radius to be $r = 25$ mm and the length of the arms $L = 100$ mm. With those values, the required thickness of the ring section to get the required end stiffness is $t = 2.8$ mm. The design using those values will meet the requirements, but will not be optimum for its compliance. Actually, from the observation of the FEM results, the proposed design is not far from this optimum – hardly any bending of the arms is visible. Checking the consistency of the results *a posteriori* simplifies the problem of

actually giving the expression for the function η that characterizes compliance losses in the arms.

Subsequently, we obtain a required length of $l = 14$ mm for the SMA wires, and a sectional area of $A = 4.9 \times 10^{-5}$ m. The volume of active material is about $V = 7 \times 10^{-6}$ m^3 for one actuator. Previously, using the theoretical setup presented in Chapter 2, we estimated the total mass of SMA to $V = 1.22 \times 10^{-5}$ m^3 for a given pre-strain $\epsilon = 2\%$ in the wires.

Some points should be discussed after this presentation of a design process as applied to an example actuator configuration. To begin with, there is no obvious path followed in the methodology. The stiffness of the frame and the estimation of the volume of SMA are considered as two different, poorly related issues. Furthermore, there are a lot of design variables, to which no real function can be attributed. An example is a compensation effect that occurs between the length of the arms and the thickness of the ring section, to achieve the required end stiffness. In addition, quantities such as the mass of the actuator should be added to the study and optimized for. Yet, the complexity of the setup again makes it difficult to understand what variables contributes to the mass, and how they contribute. Therefore, a more systematic approach is desired to bring more understanding in the setup and its design. A functional approach would allow us to relate functions in the actuator (stiffness, active part, amplification mechanism) to the performance, such as the mass of the device. A prerequisite for such an approach is the setting of performance metrics, which is the purpose of the next section. This identification should allow us to restrain the number of design variables to the most meaningful ones, as presented later in this chapter. The following sections thus set a more rigorous design methodology.

3.2 Identification of Relevant Performance Metrics

When designing actuators, different configurations can be proposed. Clearly, a set of performance metrics needs to be defined in order to compare the relative performance of each of them. The problem is to assess how well each actuator realizes the objectives. An initial view of objectives is illustrated in Fig. 3-5. The two main features of an actuator, in this context, were its empty stiffness and the amplification of the displacement of the active material. This view has motivated the design process as presented in the case of the example actuator. In addition to these features, there are other characteristics, such as impedance matching to the load, form factor, etc., that must be considered. These addiitonal features are discussed bellow.

Impedance matching. The impedance matching study is an indicator of how well the material is used. It tells how much of the material actuation capacity we make use of. This study corresponds to comparing the energy provided to the load upon actuation, and the maximum energy that the actuator could yield. In the case of an actuator working against a linear spring (stiffness K_{bias}), the work provided to the bias is expressed as

$$W_{\text{avail}} = \eta_{\text{imp}} W_{\max} \tag{3.7}$$

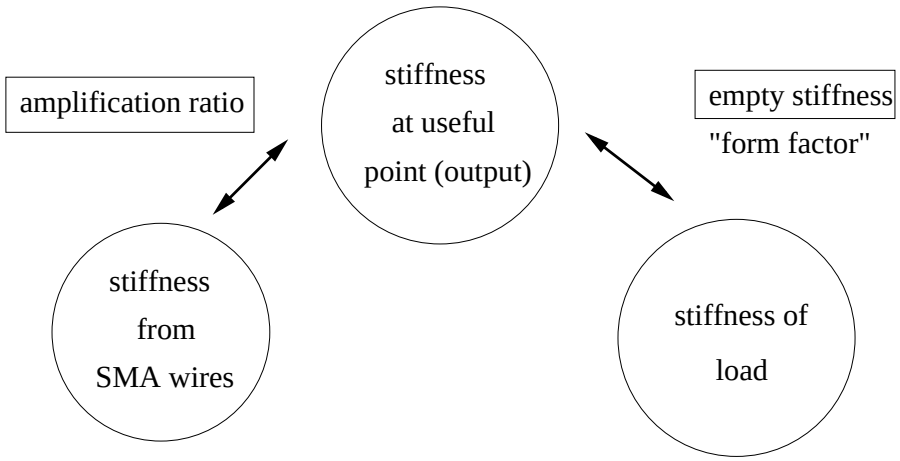

Figure 3-5: Relationships between involved stiffnesses. This view is a starting point for actuator quality assessment of the example actuator design.

where W_{avail} and $W_{\max}$ are respectively the work transferred to the load and the maximum available work the actuator can provide (Fig. 3-6), and η_{imp} is the efficiency of the transfer of work. This efficiency is a function of the ratio of the stiffness of the bias over the stiffness of the actuator. With $\lambda = \frac{K_b}{K_a}$, K_a, K_b being the stiffness of the actuator and the bias, respectively, we have

$$\eta_{\text{imp}} = \lambda(\frac{1}{1+\lambda})^2 \tag{3.8}$$

This impedance efficiency reaches its maximum for $\lambda = 1$. In this "impedance matching" case, the efficiency equals $\eta_{\text{imp}} = 25\%$. This comment holds for a linear bias, while the opportunity to use a nonlinear bias/amplification system is discussed later in this chapter. Indeed, it is conceptually feasible to design a load which characteristics results in a greater efficiency than $\eta_{\text{imp}} = 25\%$. Such a mechanism would necessitate less active material to provide actuation, although we will see this is achievable only at the expense of other performance metrics.

Mechanical transmission. The typical actuator that we are developing is composed of an active part (SMA wires) as well as of an amplification part. We need to assess the efficiency of the amplification, or transmission, mechanisms. We thus define the transmission efficiency as the ratio of the output energy over the energy put into the system, so that

$$\eta_{\text{trans}} = \frac{W_{\text{out}}}{W_{\text{in}}} \tag{3.9}$$

When we compute the total efficiency of an actuator, W_{in} is the same as the previously used W_{avail} (amount of energy available to the load). Therefore, the total efficiency is $\eta_{\text{total}} = \eta_{\text{trans}}\eta_{\text{imp}}$, which is the fraction of the maximum actuation energy that is effectively provided to the load. A part of this maximum amount of energy is lost due to the stiffness of the bias load. Another part is lost due to the energy transmission from the way the active material deforms to provide the useful energy, as Hall and Prechtl [27] discussed for the study of the bender actuator.

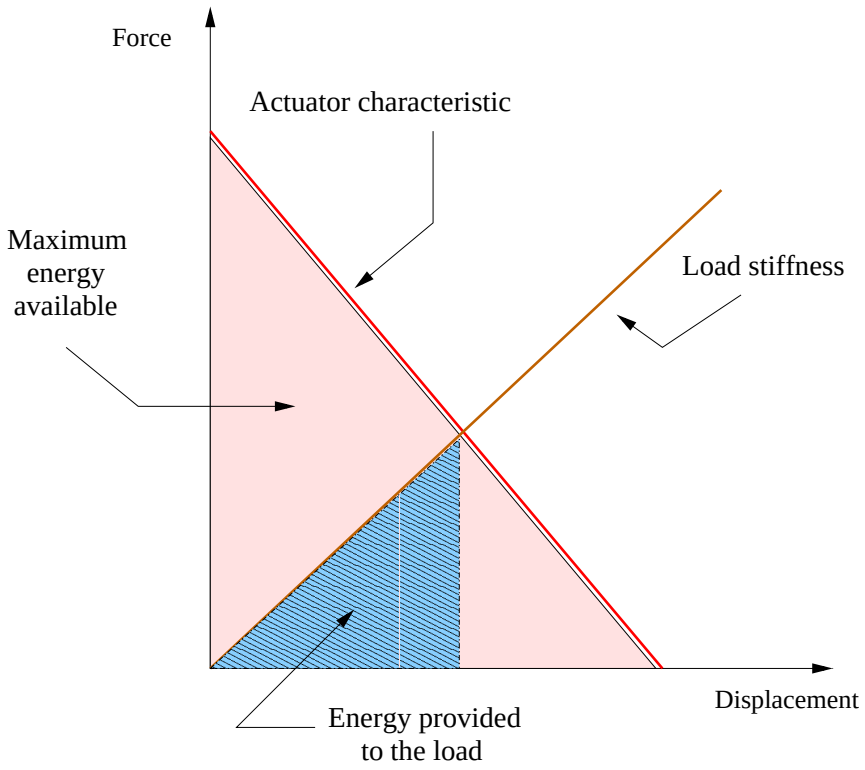

Figure 3-6: Illustration of the impedance matching concept. Maximum available energy from an actuator and energy transferred to the load.

Energy density. The energy density e (volumic density) of active materials is defined through the relation

$$V_{\text{req}} = \frac{E_{\text{req}}}{e} \tag{3.10}$$

In Equation (3.10), V_{req} is the volume of active material required to provide the right amount of actuation. We can express this energy density as a function of the pre-strain imparted to the SMA wires, as discussed in Chapter 2 (Equation 2.4). Apart from this dependency on the initial strain, the energy density is an intrinsinc characteristic of the active material. We can develop the previous equation and get more insight on the influence of the energy density and other efficiencies. From the previous efficiencies derivations, we have

$$V_{\text{req}} = \frac{1}{\eta_{\text{imp}}\eta_{\text{trans}}}\frac{E_{\text{req}}}{e} \tag{3.11}$$

Clearly, not only do we want to maximize the efficiencies defined above, but we also want to maximize the maximum energy available if that were possible. As a result, we really want to optimize the product $P = \eta_{\text{imp}}\eta_{\text{trans}}e$.

Form factor. The compactness of the device is important, therefore a good index to use is the required height of the mechanism. In other words, this question addresses the issue of how compact the amplification mechanism is. To represent the

problem, we can stress that the mechanism that provides the amplification in the previous actuator example is folded, which intuitively saves some space.

We will see when we discuss nonlinear mechanisms later in this chapter, that nonlinear amplification over a limited range is an efficient way to provide significant amplification.

Mass. The mass of the actuation device should be minimized in some way. However, Hall and Prechtl [28] showed that maximizing the mechanical efficiency introduced above makes the mass increase. Indeed, good mechanical efficiency (close to unity) requires the reacting frame stiffness to grow to infinity. As discussed by Hall and Prechtl, a mass efficiency can be defined that penalizes this trend, as

$$\eta_{\text{mass}} = \eta_{\text{trans}} \frac{M_{\text{sma}}}{M_{\text{tot}}} \tag{3.12}$$

This metrics does produce relevant results, as the piezoelectric X-frame actuator exemplifies. Yet, it fails to make a direct connection between the performance of the actuator and its mass, which is eventually the true performance we consider. Thus, the mass of the actuator itself will serve as a performance metrics.

Manufacturing. The device should be as easy to build as possible. For that reason at least, the previous actuator configuration seems not to be a very appealing one, as its manufacturing requires to work on inner surfaces for the ring and arms. This problem is mostly concurrent with the form factor issue. More complex setups could be found that provide actuation within a smaller space, to the expense of being more cumbersome to build.

Actuation time. The issue of the time for the actuator to transition from a non-actuated state to a full actuate one, and back, is considered here. This time of transition could be called a single-cycle actuation time, and is a derivative of the issue of bandwidth. However, transitions between martensite and austenite are based on very different processes: heating is done through resistive heating, while cooling is achieved mostly by forced air convection. In the application considered in this project, such a cycle is normally triggered at specific instants when the speed gets too fast. Here, it makes sense to minimize the actuation time. This time optimization issue has been poorly investigated so far. This question couples strongly with the amount of energy that has to be provided to the load. This coupling is further studied in Chapter 4.

We note here that the product P, introduced with the energy density, is divided into two parts, one part related to the setup of the actuator (efficiency with regards to the load and the amplification mechanism), and the other to the active material used (maximum energy density, an intrinsic property of such materials). Yet the two parts do interact, in particular through the constraints set on the device (time of reaction, mass,...) Hence, it will be useful to study what values of these quantities can be achieved to determine how good SMAs are at being used as actuators. This study of the performance trade-offs occurring in SMA actuators is done in Chapter 4.

In addition, an interesting study would also be to compare the performances of a given actuator to other ones, presented elsewhere. Although it is often difficult to get all the data required to fully assess a particular design, we will be able to compare X-frame actuators based on SMA or piezoelectric materials.

3.3 Choice of Functional Design Variables

The purpose of this section is to propose a set of design variables corresponding to the different functions an actuator has to meet. The significance of each of those variables should be easily identified. This choice of variables would help bring some understanding to the design process. We give below the main functions for the actuator as identified when we discussed the different performance metrics, along with the corresponding design trade-offs. Fig. 3-7 summarizes those functions.

Energy available from the active material. Usually, this quantity is a function of the operating conditions of the active sample, such as pre-load, polarization voltage (for piezoelectrics), and pre-strain (for SMAs).

Impedance matching. This metric suggests a design variable that sets the ratio of the stiffness of the active material sample with the stiffness of the load to drive. In our case, this variable has the effect of varying the volume of SMA compared to the load, thus using the energy for the wires more or less efficiently.

Mechanical efficiency. A variable affecting this performance metric controls the size (volume) of the active sample compared to the size of the reacting frame. In the following, we will use the ratio of the cross-sectional areas of the wires and the frame. The value of this variable should be sufficient to guarantee a stiff enough frame, but if too large, it results in an overweight actuator.

Amplification mechanism. The amplification ratio is a function of the geometry of the device, which would ideally be as simple as possible (characterized by a small set of parameters). This amplification will not vary the volume of active material required, yet it will affect the size of the actuator.

We should not overlook other design variables, which are related to the control of the active material sample. For instance, SMAs are often heated through resistive (Joule) heating, that is, a current is run through the wires to heat them. The required current is really a function of the diameter of the wires, while the diameter sets their resistance. Similarly, cooling is achieved by forced convection, so that the thickness of the SMA sample is an important quantity. Therefore, the diameter of the wires will also be considered as a design variable. We illustrate the two sides of the constraints put on the choice of the diameter in Appendix A (Fig. A-4). Indeed, cooling and heating are affected differently by the diameter. This issue is quite analogous to the thickness of piezoelectric stacks. If the stacks are too thick, the electrical resistivity of the medium leads to prohibitive voltage required to actuate the sample. However, there is no equivalent there to the asymmetry resulting from the cooling and heating phases of SMA actuation.

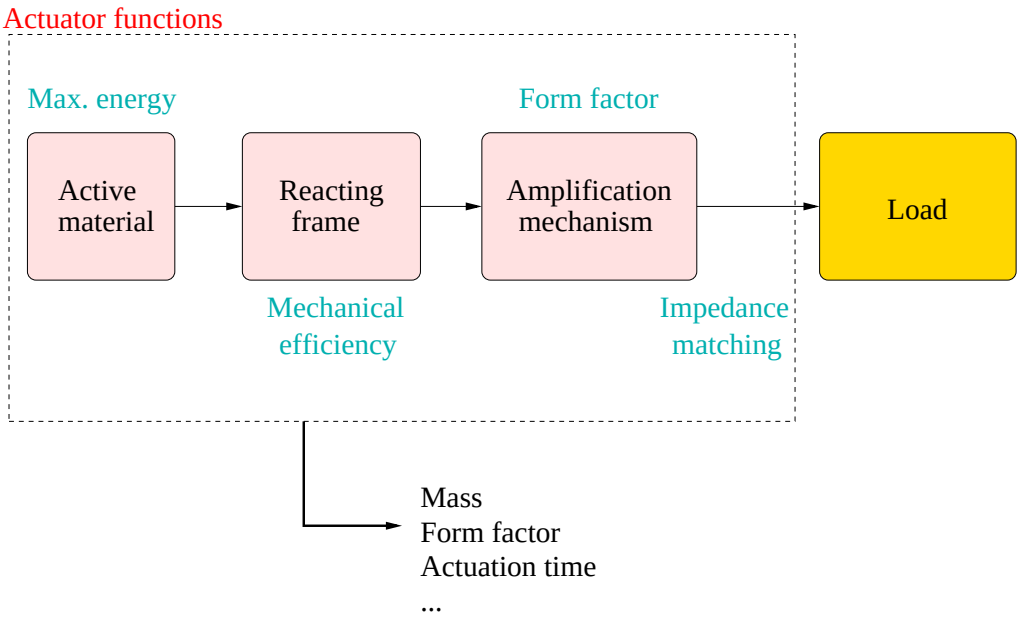

Figure 3-7: Functional flowchart for actuators. The performance metrics associated with the different elements are mentioned.

3.4 Constraints on the Design

After identifying design variables, we should set the constraints to be met. Here, typical constraints for actuation systems are listed that are likely to affect the design of actuators using SMAs.

Power. The amount of power available is an obvious constraint for actuators in general. Here, the power available has to be large enough to allow for full heating of the SMA in a reasonable time.

Response time. Any application has a time requirement associated with it, although the time for actuation is not necessary small. In the case of SMA, two response times characterize the actuation, and are based on very different principles: the heating time is a function of the input power (current), while the cooling time is mainly set by the ambient temperature and the convection coefficient.

Temperature range. The range of the transition temperatures is critical for SMAs, as those materials are driven by temperature. The transition temperatures should be set to lie outside of the ambient temperature range, so that the actuator is not inadvertently driven. On the other hand, the maximum temperature attained by the SMA sample should not be harmful for the rest of the actuator itself, nor the place where the actuator is located.

Repeatability. The device should be able to perform a significant number of cycles, while featuring a fairly constant, predictable, behavior. For SMAs, this requirement limits the amount of pre-strain imparted to the samples.

Form factor. The space available to include an actuator is usually limited, thus imposing size constraints on the device.

Mass. The additional weight of actuators usually is limited in terms of maximum weight added per unit of surface or length when the structure to actuate is a beam (*e.g.*, helicopter rotor blade).

Other constraints may be added, that are not considered here, such as the cost of the device.

The stringency of the constraints is a function of the operating conditions (satellite operation, automobile equipment, etc.), as well as of the degree of performance of the overall system. Also, the uniqueness of the systems is a recurring feature in the literature. For the most, active materials device have yet been to be proposed and implemented on mass produced systems. Active structures have been primarily developed for space systems like precision pointing observation satellites, where the performance is set very high while budget levels allow for the development and the utilization of such sophisticated technologies. The present project comes in the framework of the high-end of automotive industry or the field of racing car, which is again a class of relatively high-performance systems.

3.5 Possible Design Options

After having extracted the relevant metrics to consider in the comparison of actuation options from the illustrative example, we present here different configurations that can be of interest. We discuss them in the light of the previous comments. The concept of distributed actuation is first described. Then, the use of several small device instead of wires running along the structure is discussed. Last, the opportunity to use nonlinear actuators is studied, in order to make more of the maximum energy available to the load than a linear configuration.

3.5.1 Distributed actuation

In this case, illustrated in Fig. 3-8, the actuator is formed of two compounds, a matrix and embedded active wires. The purpose of the matrix is mainly to ensure the geometry of the whole, that is to keep the wires in place, and also to provide stiffness. The purpose of the active wires is obviously to actuate the structure. Therefore, their position, number and size must be chosen carefully.

There are some difficulties in designing such an actuated structure. First, the location of the set of wires is primarily driven by the shape that has to be reached upon actuation. Then, ideally, the weight of the whole structure should be minimized. In a very similar way as derived for local actuators, this weight optimization involves both the design of the matrix (which acts as the reacting frame in this case), and the volume of active material to use. As a consequence, models should be derived to

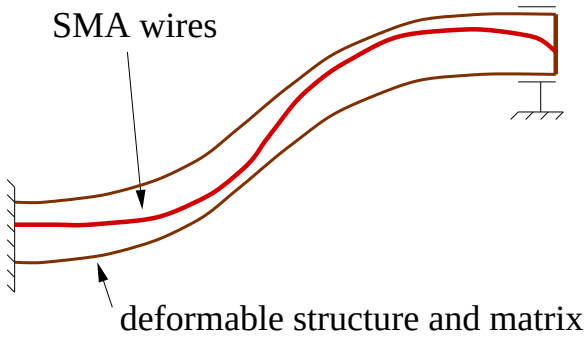

Figure 3-8: Concept of distributed actuation. A set of active wires is embedded into a matrix, the whole spanning the length of the structure to actuate.

accurately account for distributed actuation. They need to take good consideration of the coupling between the recovery force provided by the wires and the bias stiffness of the host matrix. All those issues lack reasonably tractable answers.

In the course of the present project, this design option was quickly abandoned for the reasons cited above, and others. Indeed, Hall and Prechtl [28] showed that elastic coupling actuation mechanisms are expected to be very inefficient. Another issue is that the location of the wires has to be set primarily to ensure the actuated shape will be the one expected. Consequently, this requirement forces the location of the wires to be inefficient. For instance, some active material will be put on or close to the mid-section point of the structure, thus providing no actuation. This location issue implies that more active material will be used than the minimum necessary to provide the actuation energy. An option to avoid this problem is to vary the cross-section of the active sample along the length of the active structure. This option leads to a more complicated manufacturing process.

3.5.2 Localized actuation

In this actuation concept, actuation loads are transmitted at different locations by mechanisms that push against a flexible structure, as illustrated in Fig. 3-9. This configuration is very close to the idea of "smart skin" developed by DARPA [29].

Unlike the previous case of continuous actuation, this option may offer less precision in the resulting actuated shape. However, some features make it much more appealing. The actuators are easily accessible, which implies an easier temperature control system as well as easy replacement or maintenance. Each device can be optimized independently, so that the total actuation system is likely to have better efficiency than the distributed configuration.

Therefore, localized actuation is more compelling than the distributed configuration, for both engineering and commercial reasons. However, this issue of the placement of the actuation device along the structure to deform is important. We present in Appendix B a simple rule to choose the locations and to find the stiffness of the corresponding device, using energy considerations.

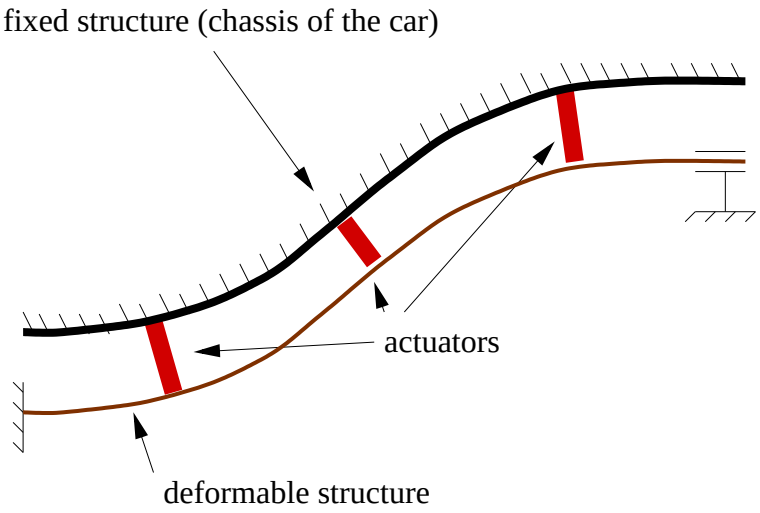

Figure 3-9: Concept of localized actuation. A set of actuators are placed at different locations along the structure.

3.5.3 Opportunity to Use Nonlinear Amplification

Here, we compare the energy output of an actuator with a nonlinear force/displacement characteristic. As mentioned earlier, we expect the impedance efficiency to have values above the maximum theoretical limit of the linear case (η_{imp} =25 %). We illustrate the study using an auto-folding device to perform the actuation and provide the minimum stiffness as required. It can be seen as a device whose internal stiffness is held constant, but the output displacement of which is not linearly dependant on the displacement of the actuation material. In other words, the amplification is not constant. A concept of such a nonlinear actuator is proposed in Fig. 3-10, where the SMA wires form an "X". They are hinged to stiff parts at two opposite sides of this "X", and linked through springs to the two other sides. The nonlinearity of the device comes from the varying amplification factor. Indeed, this factor depends on the angle between the SMA wires and the sides, thus varies during actuation.

We can compare the benefits or drawbacks of linear and nonlinear actuators. We first look at the maximum possible energy that can be achieved by a nonlinear actuator. The results are presented on Fig. 3-11. Using a nonlinear actuator with a concave characteristic function (Fig. 3-12), as for the example chosen, we see we can in principle extract more energy from the same sample of active material. This result is due to a better impedance efficiency. Indeed, nonlinear amplification mechanisms provide an internal lever effect for low displacements that improves this performance. As a result, we should expect that the volume of SMA required with this nonlinear setup equals 20% of the volume found in the linear case.

On the other hand, we now focus on the form factor of this device. The mechanism considered here is an autofolding device, so it occupies a relatively small volume. However, if we consider the required length of the frame to perform the required displacements, we get the results as summarized in Table 3.1. There, we have targeted

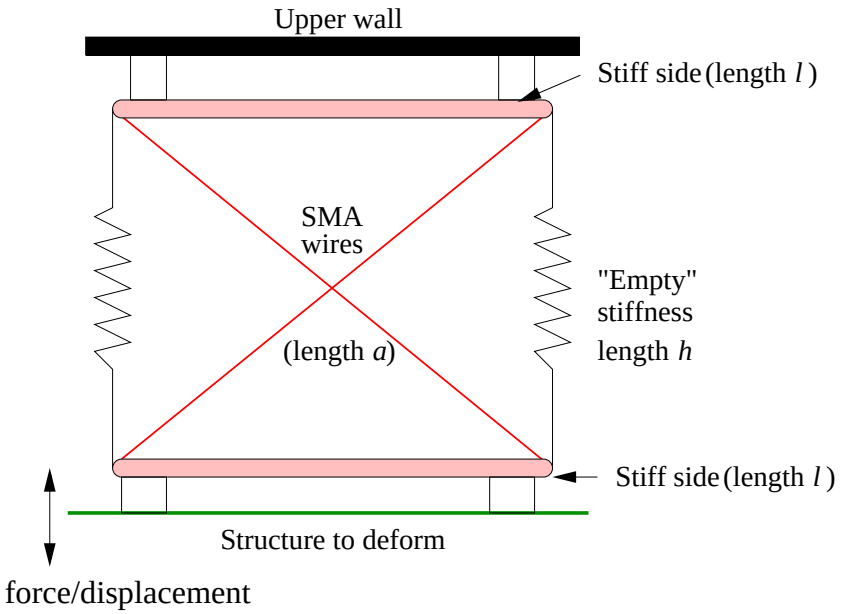

Figure 3-10: Schematic of possible nonlinear actuator.

Table 3.1: Length of the stiff sides for varying recovery strains. The nominal side height is $h = 6$ cm, the output gain is $\frac{1}{2}$.

% recovery	length
1	36 cm
2	25 cm
3	20.5 cm
4	17.5 cm
5	15 cm

a maximum gain of $g = \frac{1}{2}$, for a displacement of $d = 3$ cm. The height of the actuator is $h = 6$ cm when not actuated. The percentage recovery from the SMA wires is varied from $\epsilon = 1\%$ to 5 %. In fact, the amount of recovery strain is not known in advance, but this computation tells us that using a length $l = 10$ to 15 cm for the stiff sides may work from a geometric standpoint. This estimation is carried out without any approximation (linearization). We simply compare the heights before and after actuation given a gain, and solve for the length. The amplification mechanism obviously has to be quite large. This drawback is expected to be present every time we want to consider a nonlinear amplification. Indeed, such mechanisms require large displacements to feature a significant nonlinearity. Therefore, either we include a pre-amplification of the SMA strain, and thus complicate the design, or we use long samples of active materials, as illustrated in Table 3.1. As a result, nonlinear mechanisms are not compact in most cases.

We have stressed here a strong limitation of nonlinear mechanisms, which rely on large displacements to provide a significant increase in the energy we can get from

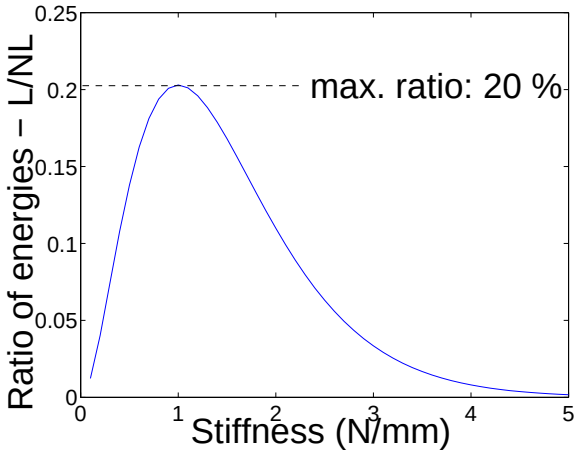

Figure 3-11: Ratio of maximum available energy. Linear over nonlinear case.

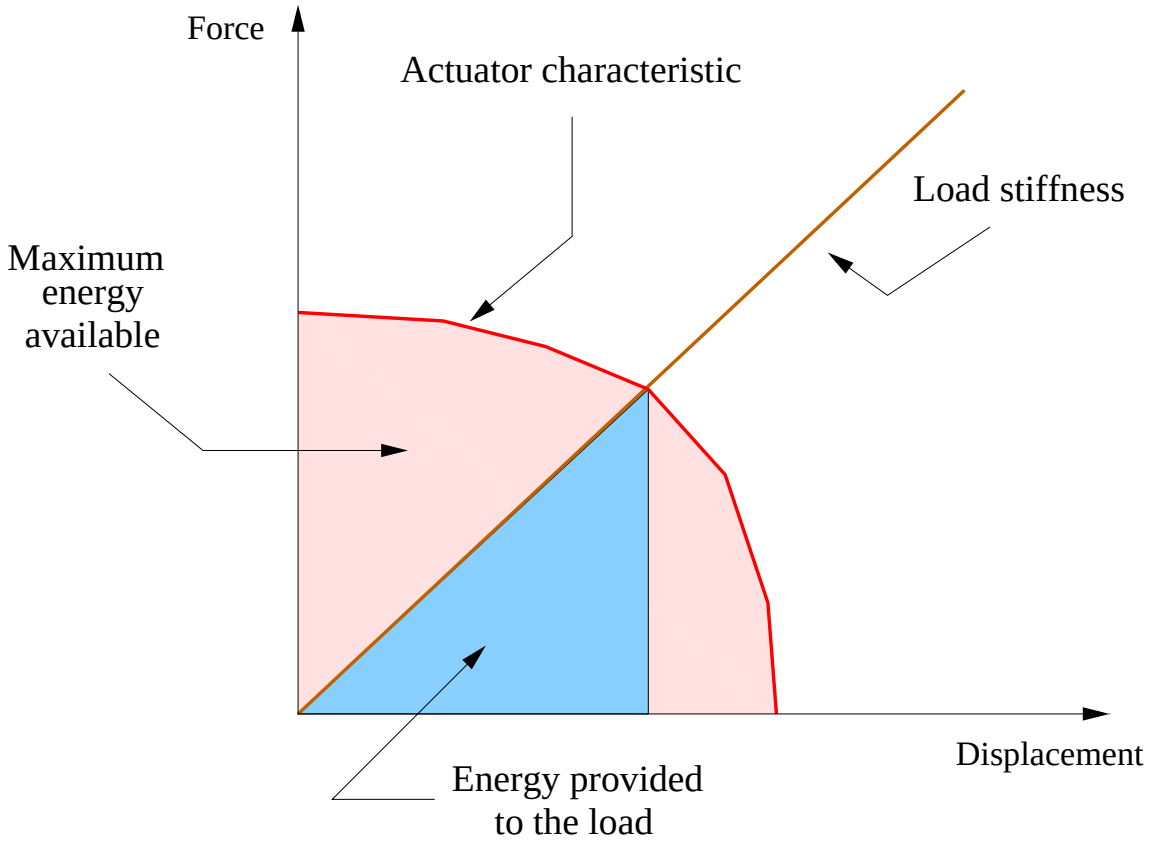

Figure 3-12: Nonlinear actuator working against a load. Characteristic of the present example.

the active material. In relation to this issue, we should note that is it also difficult to design a bias stiffness mechanism capable of withstanding the large displacements involved. Still, nonlinear amplification is good at providing large amplification. This is for instance the basic principle in the amplification of moonie actuators, in which a very flat shell is squeezed, leading to significant displacements at the top of the shell. Only the limited amount of stroke from the active material sample usually restrains the end displacements to a small range, small enough that the mechanism can be approximated as linear.

3.6 Summary

In this chapter, we illustrated the design process of an actuator. From that approach, we derived more general principles to compare different designs. Then, we applied those ideas in the comparison of distributed, local, nonlinear actuation options. The main purpose was to derive a systematic approach to actuator design. Indeed, most published papers using SMAs for active materials focus on the prediction of the behavior for a given setup, rather than on the actual design process of an actuator. This process should include efficiency considerations in addition to the specifications set for the device. Also, the correspondence between the mechanical specifications and the issue of the actuation time are rarely linked in the preliminary stage of the design process. Therefore, the purpose of this systematic approach is to assess *a priori* the overall performance of the device and improve it if possible.

Chapter 4

Trade-Off Study

In this chapter, we apply the methodology described in Chapter 3 to a specific actuator configuration. This configuration is based on a device that initially used piezoelectric stacks for actuation. After we present the corresponding model, we comment on the results. A set of good designs is identified, and we discuss their properties. The study of this set yields significant insight about the performance levels that can be reached, as well as the performance trade-offs. We use this insight to comment on the specific characteristics of SMA actuators. In particular, we show that no design can meet the requirements for our application. Therefore, the main focus of this chapter is to explain the reasons for this negative outcome, examine the possible assumptions that led us to think about using SMAs, and finally, develop a framework to help decide when SMAs can actually be worth using.

4.1 The X-Frame Actuator

In the work presented in [28] and [30], Hall and Prechtl developed a piezoelectric actuator.The piezoelectric X-frame actuator was designed to actuate flaps on helicopter rotor blades. It was required to have a sufficient bandwidth in order to perform high frequency actuation. Its weight and form factor had to allow it to be embedded into a blade. Finally, it had to be able to provide a given stroke (set in terms of flap motion), and force to react the operational hinge moment created by the aerodynamic forces on the flaps.

The methodology followed by Hall and Prechtl can be split in two parts. The first part is the identification of the needs, and definition of an actuator configuration to meet those needs.The authors focused on the notion of reacting frame. Within an actuator, this frame reacts the forces produced by the active material samples (piezoelectric stacks). In turn, the reaction of those loads allows for the efficient transmission of the SMA strains to the output after amplification. The geometry of the actuator was iteratively developed in order to use this principle of reacting frame in the most efficient way. In particular, attention was put on the form factor

and loads present within the actuator. The most efficient configuration was found to be one in which the active material samples span the length of the amplification mechanism, itself handling the role of the reacting frames. Hence, this reasoning lead to the X-frame configuration (Fig. B-1). We emphasize here that the authors used their engineering understanding of the function of an actuator to derive the X-frame configuration. This understanding is based on several principles cited in [28]. Among those principles, Hall and Prechtl concluded that actuators should not be based on coupling mechanisms to transmit the loads. Similarly, load transmission in bending or the use of flexures should be avoided. In addition, actuation device should be as simple as possible, should also be thermally stable and robust to the environment, which in the case of rotor-blade mounting, means high inertial loads and vibrations. Those principles were not precisely quantified or modeled. Therefore, this part of the design cannot be incorporated to any mathematical framework but is rather achieved through a rigorous application of design principles.

The second part of the methodology followed by Hall and Prechtl begins with the definition of a performance metric. The metric considered by those authors was the mass efficiency. This metric was discussed in Chapter 3 and will be addressed again in the following trade-off study. The choice of mass efficiency was motivated by the low mass requirements on the actuation device. Then, designs were identified that were good with respect to their mass efficiency. In addition, such designs met the mass requirements imposed for the application, although this conclusion is not guaranteed by the definition of mass efficiency.

4.2 Adaptation of the X-Frame Configuration to SMAs

We base the trade-off study for SMA actuator on the same actuator setup as the piezoelectric X-frame. Indeed, the requirements in terms of stroke and force are very similar to those imposed in the present cases. Also, similar constraints, such as the space available to fit the device, are present in the two cases.

Noticeably, the bandwidth requirements will be translated into the time for the actuator to transition from the non-actuated state to fully actuated, and back, which corresponds to a fully heating/cooling cycle. However, we can see that the bandwidth or time requirements are not fully embedded into the optimization framework as proposed in the piezoelectric X-frame actuator study. In the piezoelectric case, the bandwidth is handled as a property of the active material itself. Therefore most studies really consider bandwidth considerations as a by-product more than as a performance that could be tuned. In our case, however, dealing with SMAs, we will have to add a thermal study to account for the response time in the design.

In the following sections, we derive a model that predicts the performance of a SMA actuator with a geometry largely inspired by the piezoelectric X-frame. The main purpose is to couple material considerations with the prediction of the time

response of the actuator. The purpose is to study the performance levels that can be achieved. In addition, this model and design process should be compared to the example that was developed in Chapter 2. Here, the approach is more meaningful and systematic.

The model is partitioned into several modules (see Appendix B and Fig. 4-1):

- **A mechanical module** that assesses the performance of the actuator from a strictly mechanical point of view, as performed in the piezoelectric X-frame study.

- **An electrical module** computes the resistance of the wires, the maximum current intensity that is allowed through those wires with respect to the available power, and finally, the maximum temperature that can be reached in the wires. This temperature has to be high enough to allow for the full transformation of the SMA, from the martensite to the austenite phases.

- **A thermal module** is used to estimate the response time of the actuator. This module is pivotal, as it identifies the transfer function between the heat source and the resulting phase transition. It also captures the relation between the dimensions of the wires and the time for cooling them. Indeed, those two phenomena have to be taken into account in the estimation of the actuation time.

- Last, a module is added that checks the **feasibility** of the actuator. For instance, it makes sure that the load imparted to the frames of the actuator is not greater than the buckling load.

Such a partition of the model into modules is inspired by a Multidisciplinary Design Optimization (MDO) approach. The framework of MDO is used here to perform a design space exploration, in order to eventually be able to extract the main characteristics of SMA actuators. We are interested in identifying the limiting factors for using those actuators, understanding how the constraints are translated into bounds on the achievable performances, and ultimately, comparing SMA actuators with other actuation technologies.

4.3 Exploration of the Design Space

This section explores the design space for the modified actuator. Although it turns out no design can meet the specifications imposed, we can use the model to discuss the different trade-offs taking place. First, we identify the actuation time and actuator mass that can be achieved. Then, we visualize the constraints that are likely to become active. Last, different configurations are compared: we look at the design variables representing different trade-offs on the performances.

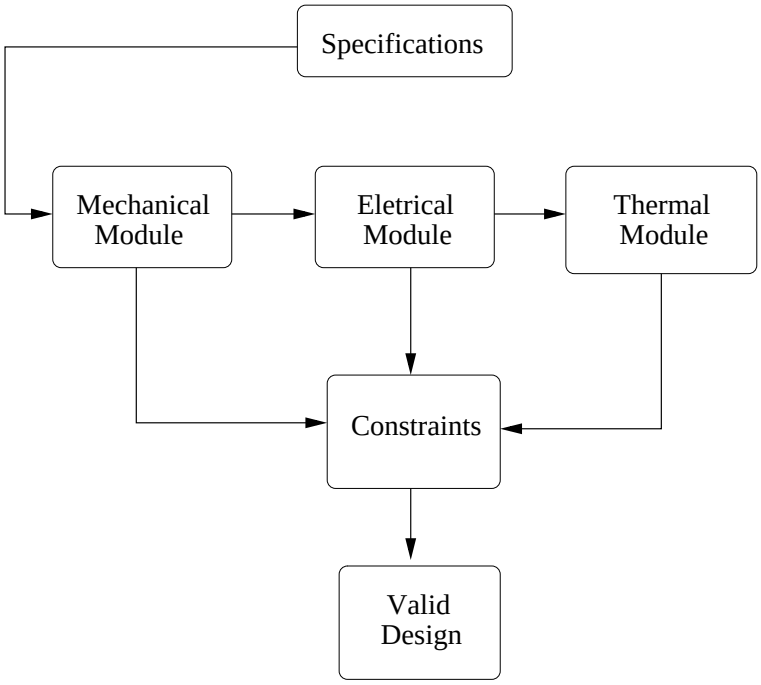

Figure 4-1: Bloc diagram of the organization of the model.

We need to scan the design space in order to identify what ranges of the design variables can lead to feasible designs, and find the values that performances metrics can take over the feasible set. However, we are faced with a multi-dimensional problem. We consider three design variables A^*, K^* and D, defined in Appendix B (Section B.1). Those design variables relate to the impedance and mechanical efficiencies for the two first ones, and D is the diameter of the SMA wires used. As for the performance metrics, we are primarily interested in the actuation time and the mass of the actuator. Thus, this problem is also a multi-objective one. Therefore, we seek to identify designs that are more relevant than others. We will use the concept of Pareto front from the framework of Multidisciplinary Optimization [31]. The Pareto front is composed of the designs for which any improvement of a performance metric reduces the performance of at least one another. In our case, we are interested in the designs for which there exists no other design with both better actuation time and mass. Such designs are thus good in terms of a particular trade-offs between their actuation time and their mass.

It is difficult to identify the Pareto front directly. Indeed, this front is really a collection of designs which are optimal for some performance trade-offs, so that trying to locate it precisely would make us run numerous optimizations problems. Our approach rather seeks at estimating the Pareto front by picking designs randomly and compare them to each other. Those designs are chosen uniformly over a certain range of the design variables, in order to get a representative subset of the design space. The following discussion considers the properties of this Pareto front. The advantage of extracting this front is to limit the discussion to designs that could

correspond to optimum designs in some situations. However, the description of those situations is of little importance. By considering a range of situations, we identify the general characteristics of SMA actuators. We will therefore have a broad picture of the performance levels and trends that we can expect from such actuators.

4.3.1 Achievable Actuation Time and Actuator Mass

We look here at the projection of the feasible designs onto the performance space. Two metrics are considered: the mass of the actuator and the actuation time. The plots in Fig. 4-2 give an idea of the values that such quantities can reached.

As a result from Fig. 4-2, the best actuation time is about $t = 15$ s, while the lower weight for the actuator is $M = 115$ g. We note that the actuation time violates the specifications for the original application in all cases. In addition, the specifications are violated even though, as pointed out in Appendix B, the estimation of the cooling time is done with a very optimistic formula.

There is a floor for the actuation time. No design among those chosen, even the unfeasible ones, can go below a certain value for the actuation time. This fact is explained by the existence of an energy gap between the two phases of SMA. Indeed, the transformation between martensite and austenite has a latent heat associated with it. The latent heat appears in the form of the variation of temperature that characterizes the transformation (Fig. 2-3). The amount of power required to perform the actuation is set by this latent heat and the mass of SMA used. The mass is a function of the energy to be provided for the active samples. Assuming we use a constant power, the energy gap to bridge in order to get full transformation increases with the amount of energy that is provided by the SMA samples, as more mass of SMA is used in that case. Therefore, the energy requirements of the application considered and the latent heat of transformation both imply the existence of a lower bound for the heating time. This minimum time can be reduced by reducing the amount of energy required from the SMA sample (equivalently the minimum mass of SMA required). In addition, we note that the cooling process contributes for a larger part of the actuation time than heating. In the shape memory effect, cooling dissipates the energy stored in the samples to overcome the latent heat of the phase transformation. Therefore, cooling time also presents a lower bound, and would be reduced as well in the case of applications requiring smaller energy levels. In the last section of this Chapter, we provide tools to estimate the dependency of the actuation on the energy requirements.

In addition, the lower part of the Pareto front seems quite horizontal in Fig. 4-2. If it were the case, the designs located at the lower left corner of the front would be designs with very little trade-off between time and mass. However, we should underscore that it is not the case. Indeed, we will see in the following sections that the mechanical efficiency increases along the front in the direction of higher mass. This increase in the mechanical efficiency implies that less SMA is used for actuation. As a result, the energy gap mentioned above is smaller as less active material is

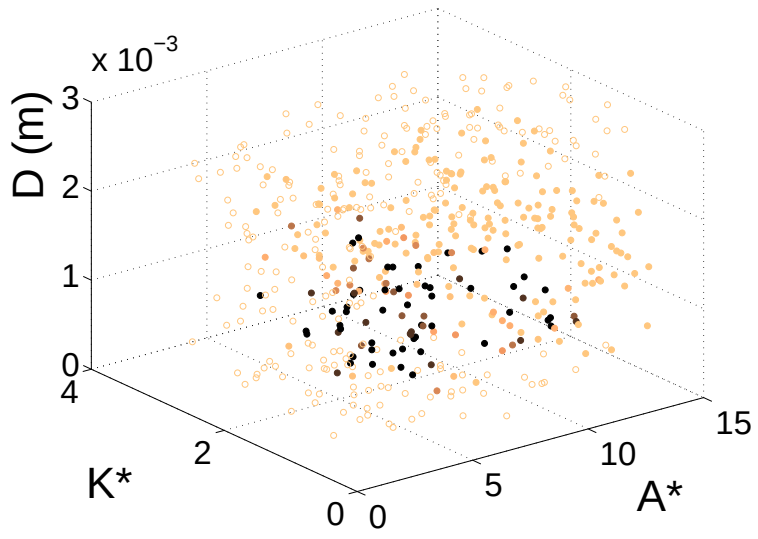

(a)

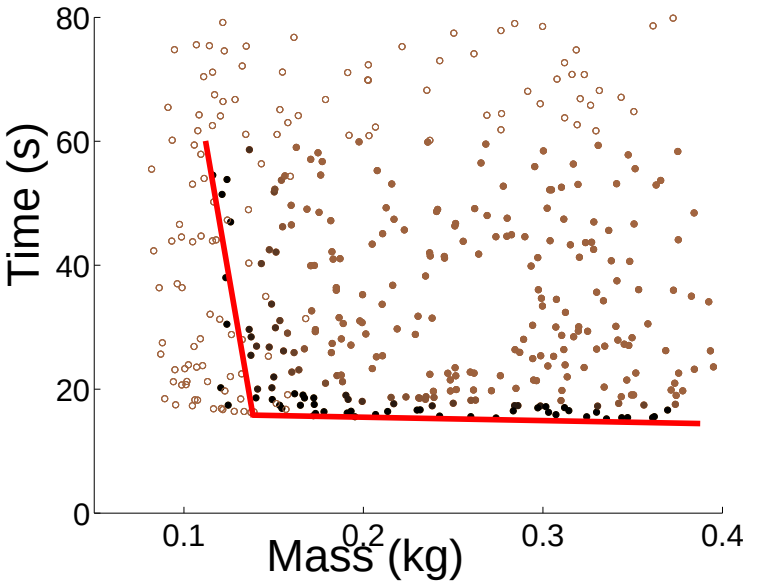

(b)

Figure 4-2: (a) View of the designs chosen. The designs that do not violate any of the constraints are marked by full dots, and the darkest dots represent the designs that are the closest to the Pareto front. (b) Projection of the chosen designs onto the performance space. This view shows the best achievable performance, for the mass of the actuator and actuation time. The red line marks the approximate location of the Pareto front.

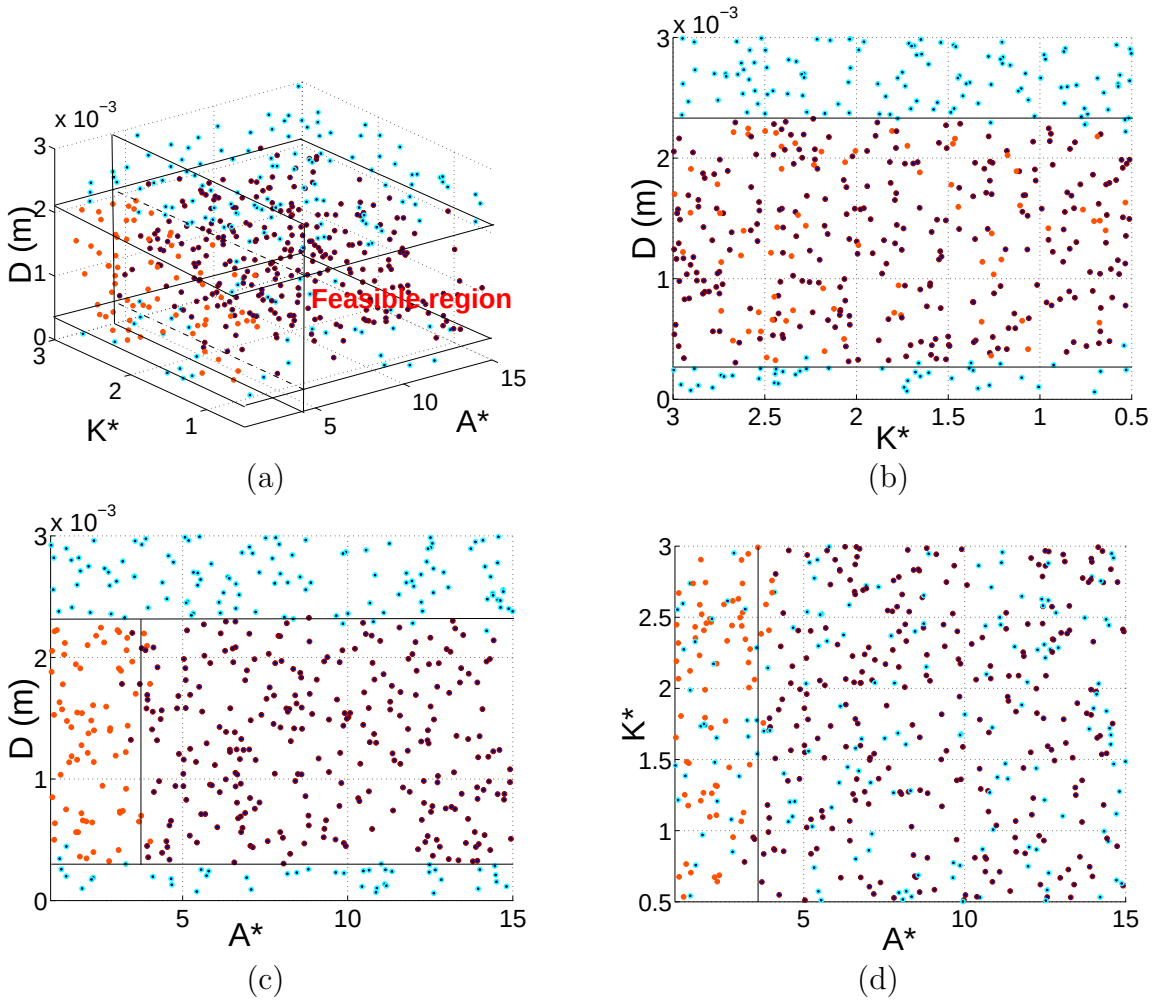

Figure 4-3: Regions where the different constraints imposed on the design are violated. (a) View in the design space. (b), (c), (d) Lateral views. We have sketched plans that delimit the feasible region and the regions where different constraints are active.

involved. Hence the actuation time should decrease. Although scaling effects hide this phenomenon, the lower part of the Pareto front is truly decreasing in the direction of increasing actuator mass.

4.3.2 Identification of Active Constraints

We can label the designs that fail to meet some of the constraints according to which ones they violate. By doing so, we map the constraints onto the design space so as to get some insight on the range of the design variables that are likely to lead to feasible designs.

We can divide quite clearly the design space with respect to those constraints, as shown in Fig. 4-3 (a). The clustering of the designs with similar properties is a benefit from the choice of the design variables, as we discussed in Chapter 3. Similarly, we

can identify a cluster of good designs on Fig. 4-2 (a).

We see that time and mass are the metrics that vary the most, and of course, really constrain the present problem. Also, the loads within the device can be such that they cause buckling of the arms. This risk of buckling imposes a minimum value for the variable A^*. The diameter is limited above by the cooling time and maximum power available. The larger the diameter, the longer the time to cool the samples back to the ambient temperature. In addition, both models used for the thermal suggest suggest an increase of the heating time with the diameter of the SMA wires (see Eqs. A.6, A.7). This variation may be due to a "bulk effect". The SME being a modification of the atomic configuration within the material, it may take place more easily in a small sample in which the modification can spread more freely.We also limit the diameter below to take into consideration the area covered by the wires. The thinner the diameter of the wires, the wider the actuator should be. We can attempt to solve this problem by placing the wires on several layers. This solution is likely to yield complex frame design, and in addition would reduce the efficiency of the convective cooling (air circulation between the layers). The effect of implementing this solution are not studied further. We should note the heating time is always much smaller than the cooling time, therefore the consequences of not looking at this option are not important in the following.

4.3.3 Study of Configurations for the Actuator

We extract three designs in order to comment on the values of the design variables with regard to the performances. First, we find a configuration that minimizes the mass of the actuator. Then, another design is chosen that minimizes the actuation time. Last, we consider a design in the lower left corner of the Pareto front as seen on Fig. 4-2. This design optimizes the sum of the actuation time and the mass. As such, its performance is a trade-off between time and mass. Then, we plot the values of the design variables and those of the performances on two radar plots (Fig. 4-5), so that we can compare them.

The minimum mass configuration corresponds to the configuration with the highest mass efficiency, as expected. This radar plot also shows that in order to reduce the actuation time, large mechanical efficiency is required. Here, this efficiency reaches $\eta_{\text{mech}} = 0.96$. It is not equal to unity only because we have bounded the variable A^* from above. Last, the impedance efficiency is kept to $\eta_{\text{imp}} = 0.25$ in all cases. The issues of time minimization and mass minimization clearly appear to compete against one another. The designs corresponding to different performance trade-offs have very distinct values for the design variables as well as for the performances.

4.4 Performance Trade-Offs

In this section, we focus on the trade-offs at the level of performances, after the previous section that looked at the evolution of the design variables. We look at the evolution of the performance metrics that were previously identified as being measures of the goodness of a design. We should expect those metrics to be coupled. This coupling is studied here. We can then compare the trends corresponding to the SMA case to other actuators. This section therefore helps define what are the specific properties that we should expect from SMA actuators.

4.4.1 Variation of Efficiencies Along the Pareto Front

Here, we look at the variations of the performance metrics along the Pareto front. These variations give a sense of the performances featured by good designs.

The graphs in Fig. 4-4 show the variation of the performance metrics along the Pareto front. The best designs in terms of actuation time are characterized by a high mechanical efficiency and low mass efficiency ($\eta_{\text{mass}} = 3\%$). On the other hand, mass optimal designs have the lowest mechanical efficiency, while being close to the maximum mass efficiency of $\eta_{\text{mass}} = 33\%$. Therefore, this study suggests that when actuation time is a requirement for an application, the mass of the device can not be minimized. Rather, mass should be traded for some improvement in the actuation time. This trade-off is not the usual way to design an actuator, and it is due to the particular characteristics of the SME.

Back to a configuration we mentioned in Chapter 3, those remarks should strengthen the case against embedding the wires. We claimed that such configurations suffered from low mechanical efficiencies. Hence, with regard to the requirement of large mechanical efficiency for time-sensitive problems, such systems are expected to require the utilization of much more active material than the theoretical minimal amount, and also have poor actuation times.

4.4.2 Comparison with the Piezoelectric Case

For the piezoelectric actuator, the optimal design was defined as minimizing the mass of the actuator only. Thus, the performance index was chosen to be the mass efficiency. It was noted with the study of the piezoelectric X-frame actuator [28] that the mass efficiency had the effect of preventing the mechanical efficiency to tend to its maximum value of $\eta_{\text{mech}} = 1$. Indeed, actuators with high such efficiency have to use strong and thus heavy reacting frames to react the loads created by the active stacks. In the case of SMA actuators, the time issue makes us force the mass efficiency to lower levels than the ideal maximum value. Therefore, SMA actuators are expected to be relatively heavy. They are indeed heavier than they could be without taking the time issue into acount.

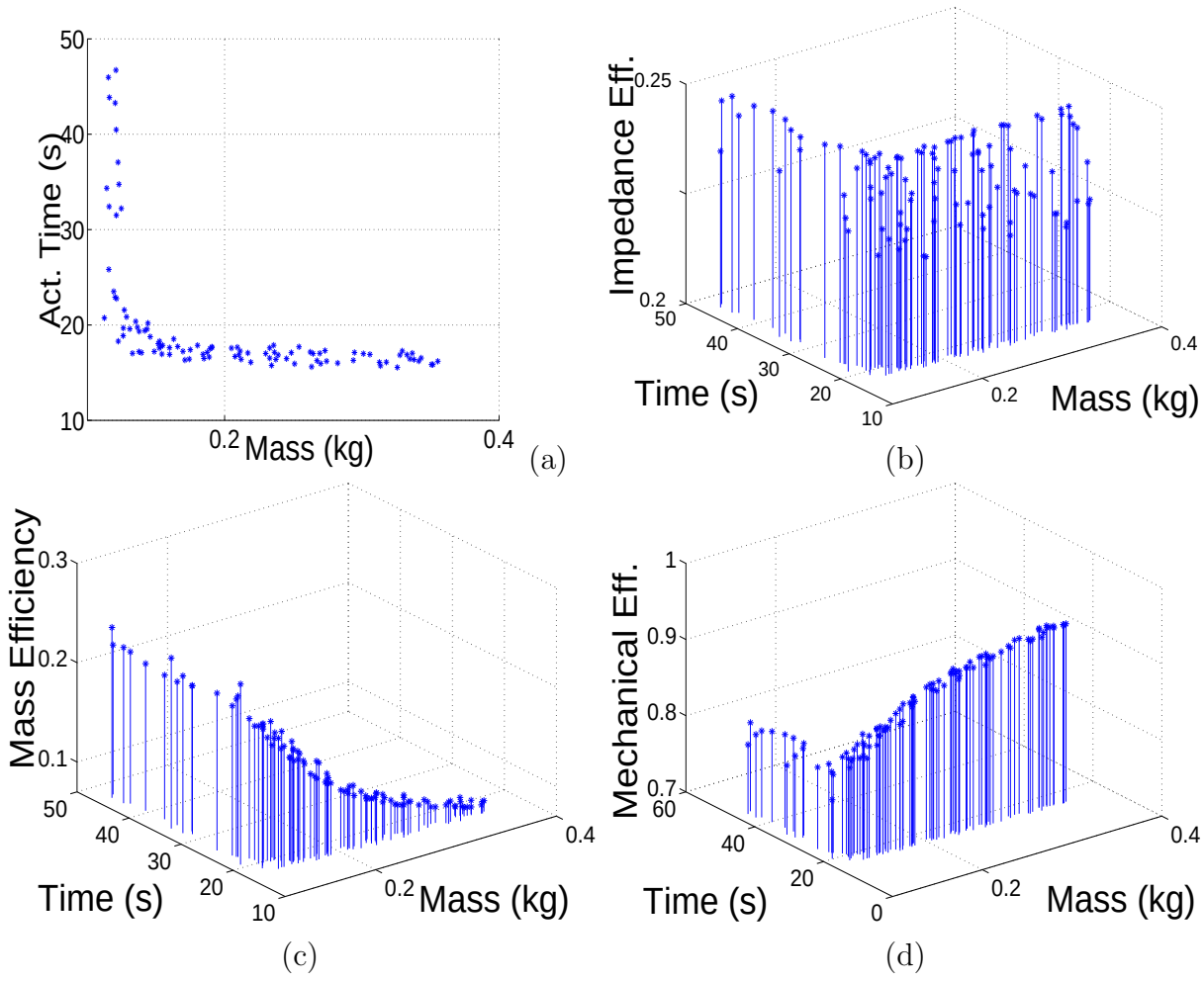

Figure 4-4: Variation of performance metrics along the Pareto front. (a) View of the performance (b) Impedance efficiency (c) Mass efficiency (d) Mechanical efficiency

However,the maximum amount of energy that SMAs can provide is still significantly higher than the energy from piezoelectric materials. As we discussed about the quantity $P = \eta_{\text{imp}}\eta_{\text{mech}}E_{\max}$, lower values of the mass efficiency do not necessary result in larger actuator mass. The much larger energy of SMA compared to piezoelectric materials can compensate for the less efficent use of active material. Therefore, the previous conclusion does not mean that SMA actuators are heavier than piezoelectric ones for the same specifications. Rather, SMA actuators should not be designed for by minimizing their mass only. Design problems should then be formulated as finding the design with the best possible mass efficiency, but with an actuation time meeting the specifications – if such a design exists. Importantly, this problem formulation invalidates the direct utilization of such graphs as the one proposed in the introductory chapter of this thesis (Fig. 1-2). This chart compares the maximum energy available from samples of different active materials or mechanisms, but they decouple this issue with the problem of other performances. Our case is an example of the false conclusions that Fig. 1-2 can lead to. In the case of the selection of active materials, such graphs as the one presented there must be completed with an in-depth identification of trade-offs on the performances of specific types active materials. In particular, the benefits of using SMAs should been downgraded. Indeed, while they theoretically provide much more energy, time-sensitive applications (even loosely so) require to trade some mass efficiency for higher mechanical efficiency. Therefore, the gain in energy density of SMAs as compared to piezoelectric materials is offset by the significant increase in the mass of the actuator.

4.5 New Tools for Selection of SMAs

In the light of the above analysis, we propose a set of tools that can be applied to assess the viability of SMA actuators for a particular application. Two such tools are proposed. One looks at the actuation time, while the second one estimates the mass of the resulting actuator. In contrast to the case of piezoelectric actuators, where the mass efficiency dominates design decisions, in the case of SMA actuators, we must generally trade actuator mass against actuation time.

4.5.1 Estimation of the Actuation Time

As explained earlier in this Chapter, shape memory alloys have to overcome an energy gap for the shape memory effect to take place. Thus, there is a minimum time for actuation. The actuation time is proportional to the amount of energy required, if a constant power source is available. As a result, designers should evaluate this minimum time before working on the details of the design. The estimation of the actuation time can be done using the equations

$$P\Delta t = mc_{\text{p}}\Delta T + m\Delta H \tag{4.1}$$

$$m = \rho_{\text{SMA}}\frac{E_{\text{req}}}{e} \tag{4.2}$$

Equation (4.1) estimates Δt, the heating time, using the translation of energy from the heating source (power P) to heating the wires (temperature increase ΔT) and the shape memory effect, represented by the latent heat ΔH. Then, taking into account the cooling conditions, we can estimate the cooling time as well. This time would normally be a function of the shape of the sample, for instance wires (with a fixed diameter), or the ambient conditions (convection, etc). When required, experimental data or a rough estimate should be used. Examples are given below in the case studies. Equation (4.2) translates the energy density of SMA (e) into an estimate of mass of SMA required (m). This formula is similar to the ones presented in Chapter 2.

In the present case, this preliminary estimation was performed. The values from Shahin [17] are used for the latent heat of transformation and the heat capacity of SMAs. The temperature increment is taken as the difference between the ambient temperature and the austenite finish temperature (full transformation), so that $\Delta T = 21$ C. In addition, we use the maximum amount of power available ($P = 2000$ W). Those conditions result in an estimated heating time of $\Delta t = 1.2$ s. Obviously, the cooling time would be larger than that. Thus, we estimate that in the best possible case, we expect difficulties in reaching the target time of $\Delta t = 3$ s. We note here that this result implies SMAs should be better for use in small systems.

4.5.2 Mass of Actuator

The second design principle that can be extracted from this thesis is the numerical value to consider for the mechanical and mass efficiencies. Mass efficiency should be optimized for only if there are very loose time requirements. However, in the more likely case that time is an issue as well, this efficiency should be released. Using lower mass efficiency would drive the mass of the actuators higher, but may improve somewhat the response time. Although it is difficult to quantify this trade-off more precisely, these comments at least emphasize the importance of using a model as exhaustive as the one sketched in Fig. 4-1. Using such models is less critical in the design of piezoelectric actuators.

At the preliminary stage of the selection of active material, a way to account for the mass efficiency release is to estimate the mass (or mass efficiency) of the actuator corresponding to ideal cases of $\eta_{\text{imp}} = 0.25$ and $\eta_{\text{mech}} = 1$. Then, the mass of active material is obtained from the energy density of SMA. Eventually, the definition of mass efficiency (Equation (3.12)) allows us to estimate the mass of the actuator, using

$$M_{\text{tot}} = M_{\text{SMA}} \frac{\eta_{\text{mech}}}{\eta_{\text{mass}}} \tag{4.3}$$

In the present case, the estimated mass of actuator would be $M_{\text{tot}} = 2.2$ kg, obtained for a mass efficiency of $\eta_{\text{mass}} = 3\%$. This value for the actuator mass is much larger than the mass that could be estimated using only energy considerations, as expected. realistic as it takes the time issue into account.

4.5.3 Case Studies

We illustrate the selection process by applying it to published works. Each of them has been taken through testing, so that we can have a good idea of how they perform. The project of an underwater biomimetic vehicle [10] is a case of actuation with antagonistic sets of wires. The project tries to achieve a frequency of $f = 5$ Hz for the device. The available power is $P = 1200$ W. The actuation task is to produce the undulation of a foil. The hydrodynamic moments and deflections involved are found experimentally, from which we can estimate the actuation energy required. In addition, the experimental history of the wire temperature shows a variation of $\Delta T = 120$ C. Assuming the actuation system can reach $\eta_{\text{mech}} = 1$, we obtain a mass of the actuation system of $M_{\text{tot}} = 20$ g. We also assume the cooling time to be of the same order as the heating time, which is consistent again with the experiences done underwater. Those values lead to an estimated maximum actuation frequency of $f = 20$ Hz. We have included the issue of probably high thermal losses in this computation only through an optimistic estimation of the cooling time. However, the setup is not capable of achieving $\eta_{\text{mech}} = 1$. Rather, similarly to the bender actuator [27], this efficiency can be at most $\eta = \frac{3}{4}$. Taking this new value gives a maximum attainable frequency of $f = 13$ Hz. Therefore, provided the mass of the actuation system is not too large, the concept is feasible. However, this result holds for the scale considered there. The scale of the system drives the energy requirements. Scaling up the device would result in an increase in the actuation time. For instance, scaling up by a factor 2 would reduce the maximum efficiency to $f = 3$ Hz, which violates the speed requirement. In addition, the pre-strains imparted to the wires are given as $\epsilon = 5\%$. This value of pre-strain is large if a lot of cycles are required (which is likely to be the case). Taking $\epsilon = 2\%$ makes the frequency drop to $f = 0.3$ Hz.

The second case on which we apply our selection tools is a micro-pump presented in [13]. It uses a SMA valve which is initially stretched through the application of a pressure differential (we assume $\epsilon = 2\%$). Upon recovery, the active layer contracts, thus producing the pumping. This device is set to pump 0.4 μL per cycle. The period of those cycles is about $t = 5$ s. This device is thus rather slow; however it has the capability of working at high pressure differentials. Here, this differential is $\Delta P = 100$ kPa. The maximum displacements of the valve are given, from which we infer the energy provided by the SMA layer. We must account for the deformation of the valve, which is not a piston so that the average displacement of the valve is less than the maximum value given. Last, we account for the cooling using a cooling time twice as large as the heating time. This experimental results provided are slightly larger. In addition, heating is achieved at a rate of $W = 2$ J during $t = 100$ μs. The frequency achievable by this device is found to be $f = 0.4$ Hz, or a period $t = 2.4$ s. This time estimation is consistent with the results provided, which show a period of $t = 5$ s.

These case studies show the consistency of the prediction of our model. It allows for a quick assessment of feasibility or achievable performances. In addition, the last example illustrates how the amount of energy can decrease the actuation time.

4.6 Summary

In this chapter, we have worked a concrete case. We have been able to draw a number of conclusions from the study of a set of particular designs. Those designs were the ones which are optimal with respect to a trade-off between actuation time and mass. The two main results are the following: in an application, the energy required from the active samples directly drives the actuation time – the lesser the energy required for the application, the fastest the response can be. Secondly, mass must be traded for time performance. Therefore, SMA actuators cannot be designed by trying to minimize their mass. SMA actuators thus have to be heavier than they could be if actuation time were not an issue. Designers must be aware of this fact, and read energy charts such as Fig. 1-2 with caution. The expected performance of SMAs should indeed be downgraded to account for this trade-off.

In addition, we have presented rules to estimate the performances or feasibility of SMA actuators for a given application. They are not original in their formulation, but rather they express specific trade-offs to account for in the design of SMA actuators. Those rules provide an estimation of such quantities as the achievable mass efficiency to use in that context. Their results give very consistent results when applied to different cases. We also note that the same set of rules would lead to decide SMA actuators are not capable of providing fast enough actuation in the original application addressed in this thesis.

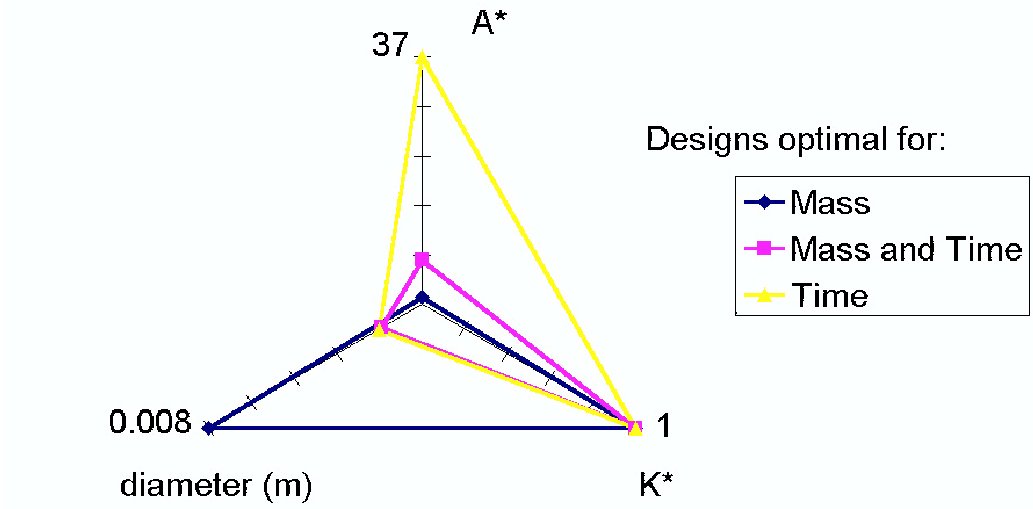

(a)

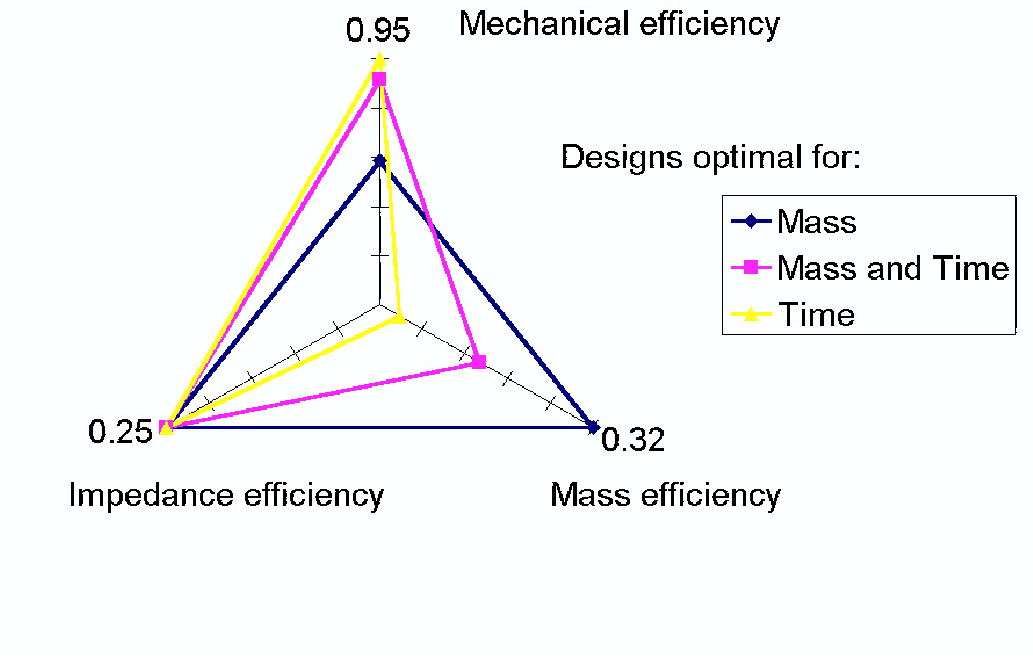

(b)

Figure 4-5: Three configurations for the actuators. Minimum mass, minimum actuation time, and "equal" trade-off case between the two. (a) Corresponding design variables, and (b) performances.

Chapter 5

Conclusion

5.1 Summary

The work presented in this thesis had the initial task of designing an actuation system for the undertray of a sports car. For this task, shape memory alloys were chosen for two reasons. First, SMAs have a high energy density compared to other active materials, and should provide enough energy for this application. Second, the required actuation time is relatively long, making SMA actuators a possible candidate. In order to propose an actuation system for this application, we presented a model for SMA actuators. This model was based on a simple estimation of the energy provided by the samples (wires). This model is original, in that it is intended to provide information that will lead to a good estimate of actuator design parameters. From this model, a rough estimation of the required quantity of active material was obtained, and led us to conclude that an SMA actuator might be feasible for our application. In addition, a deeper understanding of the shape memory effect raised some subtleties to account for in the design of SMA actuators. We refined the requirements on the actuation system accordingly.

Then, we developed a design methodology to follow for the design process. It was motivated largely from the work on a piezoeletric actuator by Hall and Prechtl [28]. Relevant performance metrics were identified, in order to define what to optimize the system for. Then, we underscored the need for choosing design variables clearly related to those performance metrics. We used those performance metrics to comment on different possible configurations for the actuation. A system composed of several linear actuators, located along the structure to be deformed, was chosen as the most promising.

We used this design methodology along with the relevant models of the shape memory effect to assemble a full, multi-disciplinary model for the whole actuation system. The results from this model highlighted the importance of coupling the mechanical problem with the thermal problem. The first conclusion from these results was that it is not possible for SMA actuators to actuate fast enough for this application. The study was then completed with the identification of limiting factors to

using SMAs in actuators. Two main ones are discussed here. First, the amount of energy to be provided by the SMA samples sets the minimum actuation time that can be achieved. This minimum value decreases with a decrease in the required energy. In addition, the mass of the actuator has to be traded for time, in order to keep the actuation time at low levels. We eventually developed rules capable of roughly estimating the minimum achievable mass and time. They were applied to our original application, as well as two other works published in the literature. Those rules consistently estimated minimum actuation time and mass levels for SMA actuation systems, and thus showed that they could offer valuable insight about the feasibility of using SMA actuators for a given situation.

5.2 Contributions

The purpose of this work was not to develop a new model for the shape memory effect. On the contrary, we used existing models, and adapted them to fit the needs of actuator design. The resulting new models made possible the adoption of a design methodology in which the two important performances, actuation time and mass, were traded off against each other. Indeed, no reference could be found where time in particular was considered as a design target, and not a by-product of a certain configuration.

Assembling this model brought significant understanding of the issues that appear with SMAs. Such materials are widely considered as potentially very advantageous compared to other kinds of active materials due to their higher actuation strain and stress. However, we showed that the generic performance levels have to be downgraded. Whenever actuation time is an issue, the mass of the device cannot be simply optimized for. Rather, the mechanical efficiency is the performance to drive as close as possible to its maximum. This outcome is obviously counterintuitive, in that implies heavy actuators. Further, there is a marked difference between good SMA designs, and good piezoelectric designs, in which the actuation frequency is relatively insensitive to the actuator design. The rules proposed to help make the decision of using SMAs are also a relevant contribution. They constitute a very useful preliminary feasibility assessment tool for future applications of SMAs. Such tools are certainly more tractable than the current exhaustive models.

Last, the design space exploration that was performed yielded very useful insight on the potential offered by SMA actuators. We mentioned in particular that they are likely to be relevant for small scale systems, such as MEMS. For those systems, energy levels are low enough that reasonable actuation times can be reached. We are less optimistic for large scale systems. This distinction was not clear in previous works. Importantly, this comment about the scale of systems also relates to this issue of reduced-scale model testing. The actuation time is indeed strongly a function of the scale of the system, therefore conclusions on the time response of scaled prototypes should be carefully scaled to the full scale case.

5.3 Recommendations

Our project was based on the application of SMAs to perform actuation for a specific application. They proved, however, not to be suitable. Other types of actuators and active material could work. In particular, the time issue seems to play a major role, even though the requirements were on the order of several seconds for full actuation. Materials with high power output, such as piezoelectrics, should therefore be considered. For such materials, we can think about using a significant amount of power, summed over a large number of high frequency cycles, to provide the required actuation authority.

In addition, material research should be pursued in order to produce active materials with high energy output, but also high bandwidth. We mentioned that different SMA compounds could have very different characteristics. The development of a broad database of such characteristics over a wide variety of alloys would prove useful. Adding some flexibility in the choice of alloy could help tailor the material to a specific application. The characterization of the active behaviors needs some further research as well.

Appendix A

Models for SMA Behavior

This appendix describes models of the shape memory effect as presented in the literature. Such models seek to capture the behavior with the maximum accuracy. However, they are too involved to be used for actuator design.

A.1 SMA Wire Working Against Spring

This example is adapted from Liang and Rogers [24]. It is intended to show a typical process proposed to capture the shape memory effect. The parameters used here correspond to the case of a copper-based SMA. Among other differences, this kind of SMA features much smaller recovery strains than Nitinol. We will get about $\epsilon = 1\%$ in the present case.

The setup of this study is presented in Fig. A-1. This setup is composed of a SMA wire that works against a spring and a constant load. It is representative of any actual actuator, as we can recognize the pre-load, load stiffness, and the dimensions of the SMA sample. In addition, SMAs are widely used in the form of wires.

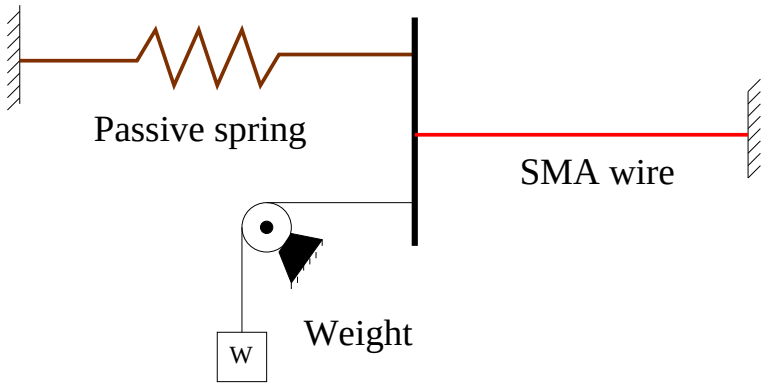

Figure A-1: Illustrative setup. SMA wire working against a weight and a spring.

A.1.1 Equations for the SME

Two equations describe the problem. Fist, the constitutive equation for the shape memory effect is

$$\sigma - \sigma_0 = E(\epsilon - \epsilon_0) + \alpha(T - T_0) + \Omega(\xi - \xi_0) \tag{A.1}$$

This equation couples the stress, strain, temperature and phase fractions of the austenite and martensite phases. ξ stands for the fraction of the martensite phase within the SMA sample, and E, α and Ω are coefficients (or tensors in multi-dimensional problems). This is the integrated version of the Tanaka constitutive relation [18]. In order to use this formula, we use a heuristic description of the variations of ξ with respect to T and σ. Several formulas exist, such as

$$\begin{aligned} \xi &= \frac{1-\xi_{\mathrm{A}}}{2}\cos[a_{\mathrm{M}}(T - M_{\mathrm{f}}) + b_{\mathrm{M}}\sigma] + \frac{1+\xi_{\mathrm{A}}}{2} \\ \xi &= \frac{\xi_{\mathrm{M}}}{2}\{\cos[a_{\mathrm{A}}(T - A_{\mathrm{s}}) + b_{\mathrm{A}}\sigma] + 1\} \end{aligned} \tag{A.2}$$

in which the first equation describes the transformation from austenite to martensite, and the second the reverse transformation. In these equations, ξ_{A} is the phase fraction of austenite at the beginning of the heating phase, and ξ_{M} the phase fraction of martensite at the beginning of cooling. In our case, assuming full transformations take place in the samples, we take $\xi_{\mathrm{A}} = 0$ and $\xi_{\mathrm{M}} = 1$. This set of equations is simply a heuristic description of plots such as illustrated in Fig. 2-3. The parameters a_{M}, a_{A}, b_{M} and b_{A} are used to fit the model to the curves. Other such descriptions exist, for instance using exponential functions instead of cosine to describe the same plots.

The second equation used to describe the shape memory effect is the description of the loading conditions. In the present case, we have

$$\sigma - \sigma_0 = \frac{kL}{A}(\epsilon - \epsilon_0) \tag{A.3}$$

where k, L and A are the stiffness of the spring and the length and cross-section area of the set of wires, respectively. The ratio $\frac{kL}{A}$ is what is called "stiffness as seen from the wires" in this thesis.

What we expect to find is the displacement of the system. As an illustration, we use here a predefined law of temperature. For convenience only, the equations for the problem are rewritten by dividing them by

$$R = 1 + \frac{AE}{kL}$$

such that $\Omega' = \frac{\Omega}{R}$ and $\alpha' = \frac{\alpha}{R}$.

The first step is to correctly initialize the problem. We assume the SMA sample is initially fully in the martensite phase, so that $\xi_0 = 1$. Then, the initial stress is given (after division of the equations by R as mentioned before) by

$$\sigma_0 = \frac{EW}{k\text{Ł} + EA}$$

We also take the initial temperature as being equal to the ambient temperature.

Next, we describe the two phase transformations. It is critical to keep track of the state of the SMA wires (phase fraction, stress and temperature) at each step. In addition, the evolution of the process should be followed closely, so that we know during the computation in what direction the transformation is going (austenite to martensite or reverse). Our choice of temperature law makes things easier.

For the transition from martensite to austenite (heating), the constitutive equations read

$$\begin{aligned} \sigma &= \alpha'(T - T_{\mathrm{M}}) + \sigma_0 && \mathrm{T_M} \leq T \leq A_{\mathrm{s}} \\ \sigma &= \alpha'(T - A_{\mathrm{s}}) + \Omega'(\xi - \xi_0) + \sigma_{\mathrm{As}} && \mathrm{A_s} \leq T \leq A_{\mathrm{f}} \\ \sigma &= \alpha'(T - A_{\mathrm{f}}) + \sigma_{\mathrm{Af}} && \mathrm{A_f} \leq T \end{aligned}$$

These expressions should produce continuous variations of the stress and phase fractions, hence the introduction of quantities such as σ_{As} to connect the problems that are described by parts (see [22]). Similar expressions hold for the reverse transformation. The initial conditions are the state of the SMA sample at the instant when the temperature starts decreasing.

It should be noted that this formulation of the problem makes us solve for the stress. Indeed, when using the expression mentioned above for ξ, we see that each of the equations are really implicit equations in the stress.

A.1.2 Results and Discussion

We plot the temperature history and the corresponding states. In addition, we can deduce from those the strain ϵ in the SMA wires, through the relation describing the load.

This procedure to capture the SME is a typical one, in the sense it uses a constitutive relation for the effect, then adds a description of the loading conditions. This example shows that this formulation leads in an implicit definition of the stress recovered during actuation. The recovery strain is found by solving for the stress in the above equations.

This method is clearly quite involved. A major drawback is that it involves many coefficients which have to be identified. One issue related to the coefficients is that they differ a lot from one alloy to the other. There exists no database that collects those data. Another issue is that other models exist to capture the SME, but they use different sets of coefficients. As a consequence, it is often difficult to compare the prediction of two different models when there is little correspondence between their coefficients or this correspondence is not known for the alloy of interest.

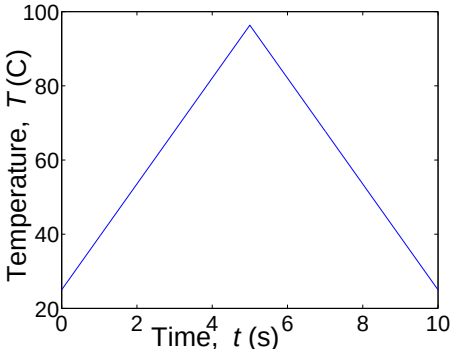

Figure A-2: Temperature law imposed on the wires.

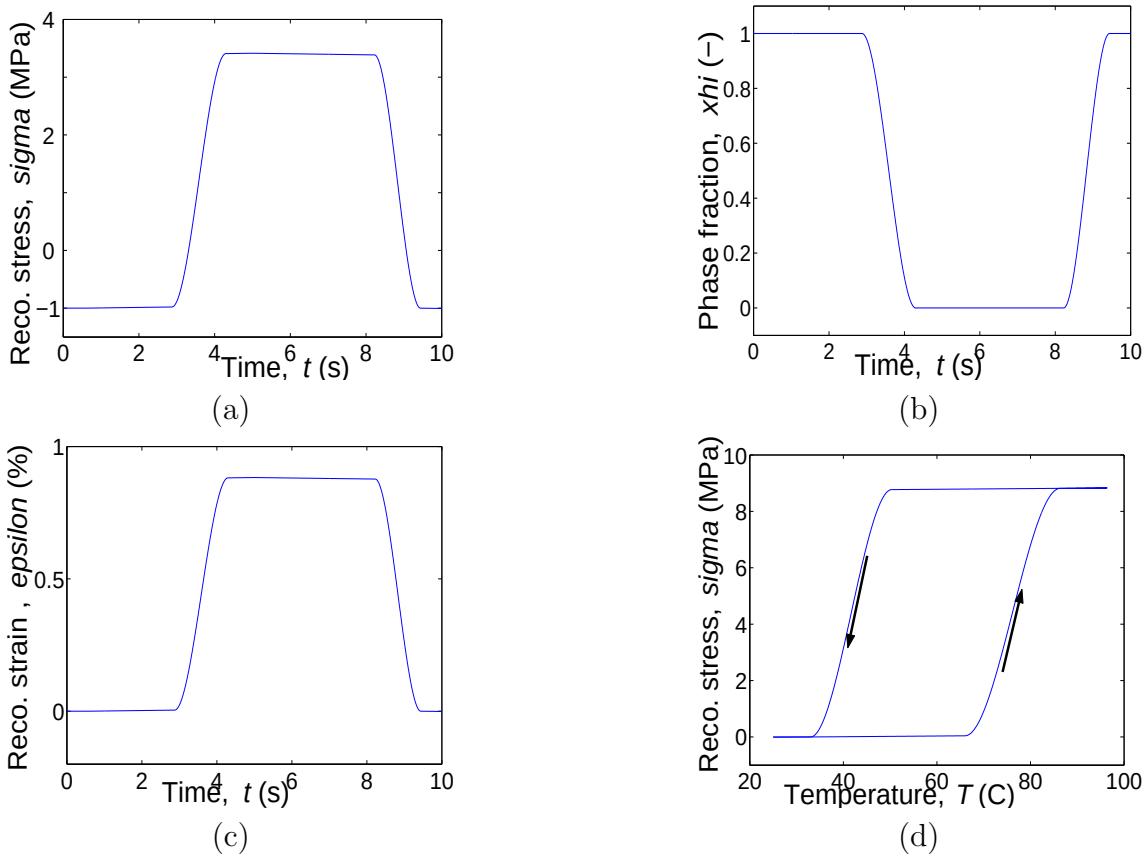

Figure A-3: With the temperature law imposed, histories of resulting stress (a), martensite phase fraction (b), and recovery strain (c). (d) Stress-temperature characteristic of SMAs under the same conditions.

A.2 Estimation of Actuation Time

Two heuristic thermal models are introduced here. The first one is used to compute easily the time response of the SMA sample, and is taken from Waram [14]. It consists of formulas that estimate the heating and cooling times for SMA wires. In those formulas, the diameter D is in millimeters, and the intensity I in Amperes.

- **Update of transition temperatures**. σ is the maximum stress in the wires, and should be estimated beforehand. From the behavior of shape memory alloys, the transitions temperatures vary linearly as a function of sigma, so that

$$T_{\mathrm{Af}} = T^0_{\mathrm{Af}} + \frac{\sigma}{C} \tag{A.4}$$
$$T_{\mathrm{Ms}} = T^0_{\mathrm{Ms}} + \frac{\sigma}{C} \tag{A.5}$$

- **Time constants J_{h} (heating), J_{c} (cooling)**. Heuristic formulas are given in Waram [14]. The proposed form is

$$J_{\mathrm{h}} = 12.06 + 12.418D^2 \tag{A.6}$$
$$J_{\mathrm{c}} = 13.25 + 18.706D^2 \tag{A.7}$$

  or in case of moderate forced convection,

$$J_{\mathrm{h}} = 6.72 + 3.922D^2$$
$$J_{\mathrm{c}} = 4.88 + 6.116D^2$$

  where the time constants J_{h} and J_{c} are in seconds, and the diameter D is in millimeters. The constants in these equations were experimentally determined by the author of [14]. These equations are given as approximations of the time constants. It is important for our model that they account for variations of the wire diameters.

- **Time of heating and cooling**. Reference [14] also gives formulas to estimate the time of the full transition of the wires, from martensite to austenite and back as, respectively,

$$t_{\mathrm{h}} = J_{\mathrm{h}} \cdot \ln\left(\frac{T_{\max} - T_{\mathrm{amb}}}{T_{\max} - T_{\mathrm{Af}}} + 121.23\frac{D^4}{I^2}\frac{T_{\max} - T_{\mathrm{amb}}}{T_{\max} - T_{\mathrm{Af}}}\right) \tag{A.8}$$
$$t_{\mathrm{c}} = J_{\mathrm{c}} \cdot \ln\left(\frac{T_{\mathrm{Af}} - T_{\mathrm{amb}}}{T_{\mathrm{Mf}} - T_{\mathrm{amb}}} + \frac{28.88}{T_{\mathrm{Ms}} - T_{\mathrm{amb}}}\right) \tag{A.9}$$

An alternative thermal model is given by Lagoudas, Shu *et al.* [23]. This second model is based on the heat equation, which is solved to compute the temperature in the wires along time. We will use this model to visualize the temperature response of the actuator when a current is applied to the wires.

- The governing equation for a one-dimensional heat conduction problem is

$$C_{\mathrm{v}}(T)\frac{\partial T(t)}{\partial t} = -\frac{4h(T,D)}{D}[T(t) - T_\infty] + \rho J^2 \tag{A.10}$$

  where C_{v} is the heat capacity, J the current density, ρ the electrical resistivity of the SMA, D the diameter of the wires, and $h(T,D)$ the heat convection coefficient ($\approx$ 30-40 W/m^2/K in still air, assumed 10 time greater for forced convection).

- The dependence of C_{v} on T is given by Reference [23] as

$$C_{\mathrm{v}}(T) = C_{\mathrm{v}}^{0} + q\frac{\ln(100)}{|T_{\mathrm{Ms}}^{0} - T_{\mathrm{Mf}}^{0}|} \cdot \exp\left(-\frac{2\ln(100)}{|T_{\mathrm{Ms}}^{0} - T_{\mathrm{Mf}}^{0}|}|T - \frac{T_{\mathrm{Ms}} + T_{\mathrm{Mf}}}{2}|\right)$$

$$T_{\mathrm{Mf}} \leq T \leq T_{\mathrm{Ms}} \qquad \text{austenite to martensite} \tag{A.11}$$

$$C_{\mathrm{v}}(T) = C_{\mathrm{v}}^{0} + q\frac{\ln(100)}{|T_{\mathrm{As}}^{0} - T_{\mathrm{Af}}^{0}|} \cdot \exp\left(-\frac{2\ln(100)}{|T_{\mathrm{As}}^{0} - T_{\mathrm{Af}}^{0}|}|T - \frac{T_{\mathrm{As}} + T_{\mathrm{Af}}}{2}|\right)$$

$$T_{\mathrm{As}} \leq T \leq T_{\mathrm{Af}} \qquad \text{martensite to austenite} \tag{A.12}$$

  where $q = 0.0618\ \mathrm{J} \cdot \mathrm{mm}^{-3}$ is a constant.

The thermal equation is solved for using a predefined law for the current density. The current is chosen to be at the maximum value allowed by the power requirements. This current is applied over a given duration, and the heat equation is solved for during this period of time. Then the cooling equation is solved over another given period. The duration of each period should be long enough to allow for full transitions in the wires, that is the temperature should range the whole range of transformation temperature (T_{Mf} to T_{Af}).The results of this model have been compared to those reported in DeWeck and Miller [32], showing good matching.

We present in Fig. A-4 a result obtained using this model. For a given set of requirements, we vary the diameter of the SMA wires used. The same power is used throughout. Heating is assumed to stop when the wires reach the full austenite state (complete transformation). The difference between the heating and cooling phases clearly appear. By reducing the diameter of the wires, the resistance of the wires increases, thus the heating time increases as well. On the other hand, cooling is improved. According to those comments, we should expect that feasible designs will be located on a strip of the diameter design variable. This strip would be the range of the diameter that allows for completely heating the wires as well as fast enough cooling. Fig. 4-3 confirms those comments.

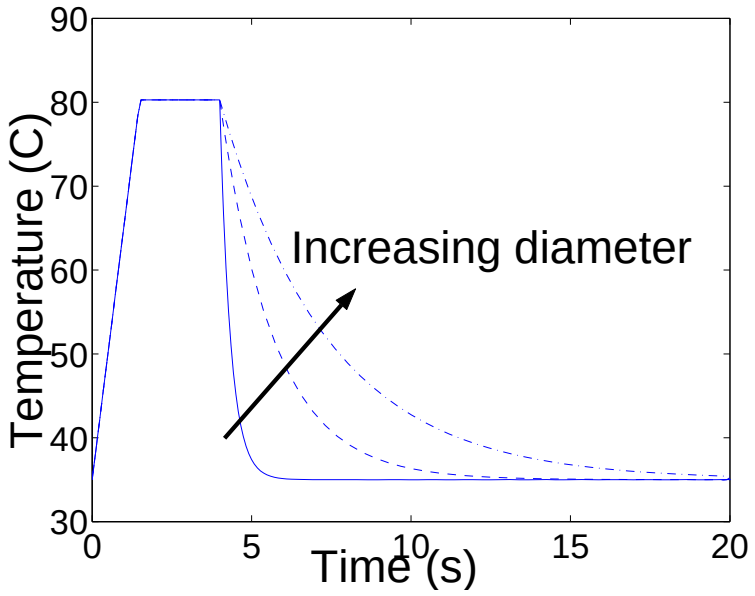

Figure A-4: Temperature in the wires. The current is constant during $t = 4$ s, then switched off. The conditions are $T_{\text{amb}} = 35$ C, and convective cooling is used.

Appendix B

Definition of Modules for the SMA X-Frame Actuator

B.1 Geometry, Setup, Design Variables

The configuration of the actuator is presented in Fig. B-1. The device features two arms, with SMA wires spun around them. At the bottom of the device, a base allows the arms to rotate, while the useful force and displacements are taken at the top. The end of the two arms are connected one to the underbody of the car, the other one to the flexible structure. The details of the hinges are not studied here.

The geometry, hence the amplification factor, is determined by the sole geometric angle θ. In order to characterize the device, the length of the arms and the wires (l_f, l_s respectively), as well as their respective cross-section areas (A_f, A_s) have to be determined. The design variables for this configuration are taken as suggested in Chapter 3. In addition to θ, we add the ratios $A^* = \frac{A_\mathrm{s}}{A_\mathrm{f}}$ and $K^* = \frac{K_\mathrm{s}}{K_\mathrm{f}}$. These ratios are chosen for their direct reference to the impedance and mechanical efficiencies. Last, the thermoelectrical problem is driven by the diameter of the SMA wires D, through which a current I is applied.

The specifications on the device are set in terms of force and displacements required at the top of the device. The influence of the corresponding amount of energy, mainly on the actuation time , is discussed in Chapter 4. In terms of the constraints, we present them as well as the way to take them into account in Chapter 3.

B.2 Mechanical Model

The mechanical model is derived essentially from the piezoelectric X-frame actuator study. It is presented here in the same way the computation is implemented, in order to show the progression of the computation. However, this progression is also very close to following a functional approach, as we will identify most of the steps with

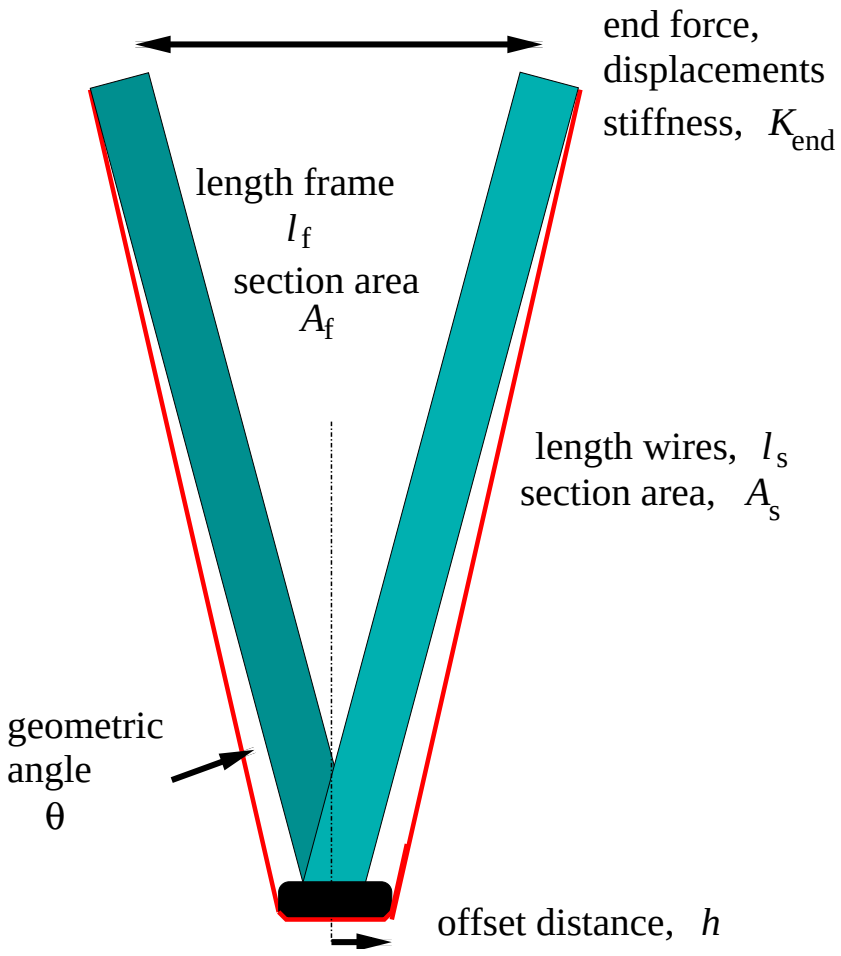

Figure B-1: Sketch of the present actuator configuration. Side view.

a very precise function (or performance) of the actuator as it was recommended in Chapter 2.

- **Frame area** A_f. From the expression of the output stiffness, given a value of A^* and an impedance efficiency, Af is computed from

$$A_f = 2\frac{K_l}{K^*}\left(\frac{l_s}{E_a \tan(\theta)^2 A^*} + \frac{l_f}{E_s \sin(\theta)^2}\right) \tag{B.1}$$

  In this formula, we use the stiffness of the device composed of the frames and wires. In addition, we factor out A_f by using the definition for A^*. As A^* is a design variable, this procedure allows us to ignore A_s at this step.

- **Wires area** A_s. The choice of A^* (related to maximum mechanical and mass efficiencies) and the previous computation of the area of the frames lead to

$$A_s = A^* A_f \tag{B.2}$$

- **Actuator empty elongation** q_f. q_f is obtained from the geometry of the X-frame as

$$q_\mathrm{f} = 2 \cdot \frac{l_\mathrm{s}}{h}(1 - \epsilon/2)\epsilon l_\mathrm{s} \tag{B.3}$$

  This formula translates the strains within the wires into displacements at the top of the device. The strain is taken as being $\epsilon = 2\%$.

- **Actuator stiffness** K_end. The expression of output stiffness, along with previously computed values of areas, gives

$$K_\mathrm{end} = \frac{1}{2}\left(\frac{l_\mathrm{s}}{E_\mathrm{a}\tan(\theta)^2 A_\mathrm{s}} + \frac{l_\mathrm{f}}{E_\mathrm{s}\sin(\theta)^2 A_\mathrm{f}}\right)^{-1} \tag{B.4}$$

  This formula is the expression for the stiffness of the device. We have already used a version of it (Eq. B.1).

- **SMA strain energy** W_e. This performance is the maximum energy available from the SMA wires (there are two sets of wires per actuator). It is the total energy resulting from the contraction of the wires, and is expressed as

$$W_\mathrm{e} = 2 \cdot \frac{1}{2} E_\mathrm{a} \epsilon^2 A_\mathrm{s} l_\mathrm{s} \tag{B.5}$$

- **Mechanical efficiency** η_{mech}. This efficiency is the efficiency of the conversion of the energy from the wires into energy available to the load. Its definition leads to

$$\eta_\mathrm{mech} = \frac{\frac{1}{2}K_\mathrm{end} q_\mathrm{f}^2}{W_\mathrm{e}} \tag{B.6}$$

- **Mass efficiency** η_{mass}. As we have computed all the lengths previously, we can estimate the mass of active material and total mass of the actuator. By definition, the mass efficiency is then

$$\eta_\mathrm{mass} = \eta_\mathrm{mech} \frac{M_\mathrm{SMA}}{M_\mathrm{tot}} \tag{B.7}$$

- **Energy output** W_a. This performance is the total amount of energy provided to the load, and is expressed as

$$W_\mathrm{a} = W_\mathrm{e} \eta_\mathrm{mech} \eta_\mathrm{imp} \tag{B.8}$$

  This expression simply rewrites the definitions of the impedance and mechanical efficiencies.

- **Energy output density** U_a. The energy output density is the energy provided to the load per unit of mass of the actuator. By definition,

$$U_\mathrm{a} = \frac{W_\mathrm{a}}{M_\mathrm{tot}} \tag{B.9}$$

- **Scaling factor** λ. Once a design has been completed at the scale given from the initial choice of the length of the SMA wires, the device is scaled such that the energy output after scaling equals the energy that is required by the application. This length scaling factor λ is thus computed according to

$$\lambda = \left(\frac{E_{\text{req}}}{W_{\text{a}}}\right)^{\frac{1}{3}} \tag{B.10}$$

  The scaling factor translates the scale on the volume to a scale on lengths. Indeed, the ratio $\lambda_0 = \frac{E_{\text{req}}}{W_{\text{e}}}$ has the dimension of a volume (m^3), thus in order to scale this volume, lengths should by multiplied by λ as given above.

- **Scaling of lengths, areas**. All the dimensions are scaled by multiplying all the lengths by λ. This procedure preserves the geometry of the device, but tunes its energy output to match the requirements.

In addition, a bias is added to the device. It serves at storing the energy during actuation, and restoring it afterwards by stretching back the SMA sample to their original length. The mass of this bias is computed from Ashby [9]. We assume the bias mechanism takes the form of a steel leaf spring, taking a U-shape and placed outside of the device.

B.3 Electrical Model

The volume of active material has been determined in the previous section. The power will be assumed as taken equal to the maximum available power, hence what we compute in the module is really the operating voltage required. The Joule heating is also modeled using a heuristic formula, taken from Waram [14]).

- **Resistance of wires** R. The number of wires to consider (n) is estimated from cross section area of SMA required in previous part, divided by area for a single wire. The wires are then connected in parallel. Therefore, the resistance of the set of wires is

$$R = \rho \frac{l_{\text{s}}}{n\pi D^2/4} \tag{B.11}$$

- **Current** I. The maximum current that can be passed through the wires is computed by taking the maximum available power P. By definition,

$$I = \sqrt{\frac{P}{R}} \tag{B.12}$$

- **Voltage** V. This quantity is the voltage between the heads and the base of the actuator. It is shared between the different wires, so that

$$V = \rho \frac{l_{\text{s}}}{\pi D^2/4} I \tag{B.13}$$

- **Maximum temperature** attained by the wires due to Joule heating (not reached). This maximum temperature would be the final temperature if the current previously computed was maintained constant over a large period of time. If this temperature is lower than the maximum transition temperature (computed later in the thermal module), then the shape memory transformation is not complete. In that case, we do not make full utilization of the SMA, therefore this case is avoided. Those heuristic formulas are taken from Waram [14]. They read

$$T_{\max} = 16.383\frac{I}{D} + 3.987\left(\frac{I}{D}\right)^2 \tag{B.14}$$

or, in the case of moderate forced convection,

$$T_{\max} = 4.928\frac{I}{D} + 1.632\left(\frac{I}{D}\right)^2$$

The diameter D in these equations is in millimeters. We take the formula corresponding to still air conditions (Eq. B.14). In this case, thermal losses are the smallest. Indeed, we consider that we use the SMA samples in the most efficient conditions so as to provide a conservative estimation of actuation time.

B.4 Thermal Model

The thermal model is presented here. First, we mentioned in the description of the SME that the transition temperatures are stress dependant. Then, we need to estimate the stress that resides within the wires. The second step is to actually estimate the time of cooling and heating of the set of SMA wires.

B.4.1 Stress Dependency

The transition temperature are related to the stress in the SMA wires through

$$T_{\mathrm{Af}} = T^0_{\mathrm{Af}} + \frac{\sigma}{C} \tag{B.15}$$

$$T_{\mathrm{Ms}} = T^0_{\mathrm{Ms}} + \frac{\sigma}{C} \tag{B.16}$$

In these expressions, T_{Af} and T_{Ms} are respectively the temperature for the end of the austenite transformation, and the one for the start of the martensite formation. They both correspond to the actuated state of the samples. Thus, the stress σ is really the total recovery force produced by the wires.

In order to estimate this stress, we can apply a reverse-engineering procedure. From the requirement, we know the amount of energy given to the load by the actuator. This energy is translated into energy provided by the SMA wires using the impedance efficiency. This impedance efficiency is indeed available as one of the design parameters through the variable K^*. From there, as all lengths and cross-sections have been determinated beforehand, we get the value for the stress.

B.4.2 Actuation Time

The time for heating and cooling are estimated using the explicit formulas taken from Waram [14]. To improve the cooling time, the time constant given for still air conditions is multiplied by a factor 10. This choice corresponds to an over-optimistic estimation of convective cooling. Indeed, the speed of the cooling flow cannot be to large for two reasons. First, the actuators are located in a space with limited flow stream. Also, the convection is always present, therefore if it were large, there would be a significant amount of heat losses during the heating process.

Thus, the equations used are as follows.

- **Update of transition temperatures**. σ is the maximum stress in the wires, as obtained from the mechanical module, and is a function of η_{imp} mainly. Eqs. B.15 and B.16 are used for the computation of the transition temperatures as a function of σ.

- **Time constants J_h (heating), J_c (cooling)**. As in Appendix A, but improving the cooling time constant by an arbitrary factor 10 (D in millimeters):

$$J_\mathrm{h} = 12.06 + 12.418D^2 \tag{B.17}$$
$$J_\mathrm{c} = (13.25 + 18.706D^2)/10 \tag{B.18}$$

  where the time constants J_h and J_c are in seconds.

- **Time of heating and cooling**. Again, we estimate the heating and cooling times as, respectively,

$$t_\mathrm{h} = J_\mathrm{h} \cdot \ln\left(\frac{T_\mathrm{max} - T_\mathrm{amb}}{T_\mathrm{max} - T_\mathrm{Af}} + 121.23\frac{D^4}{I^2}\frac{T_\mathrm{max} - T_\mathrm{amb}}{T_\mathrm{max} - T_\mathrm{Af}}\right) \tag{B.19}$$
$$t_\mathrm{c} = J_\mathrm{c} \cdot \ln\left(\frac{T_\mathrm{Af} - T_\mathrm{amb}}{T_\mathrm{Mf} - T_\mathrm{amb}} + \frac{28.88}{T_\mathrm{Ms} - T_\mathrm{amb}}\right) \tag{B.20}$$

B.5 Comments on the Reliability of the Model

The mechanical model is based on the work by Hall and Prechtl [28]. These authors observed experimental results very consistent with their performance predictions. Some checks have been done on the value computed for such quantities as the energy available. The strain energy from the SMA wires is given by most publications to located within the range: $E = 1$ to 10 J/cm^3, while the value chosen for the prestrain $\epsilon = 2\%$ and the model of energy used give a value of about $E = 2.7$ J/cm^3.

As for the thermal model, Waram [14] provides no information about the range over which the formulas are valid. Yet, it was possible to compare the predictions with some experimental results obtained in different publications, and the results from the formulas adopted here appeared to be conservative, each time. The second

reference from which we took formulas for the thermal formulation [23] gives a model with little correspondence with the previous expressions. Again, the predictions from this model were compared to published experimental results (in particular, DeWeck and Miller [32]) and there was good agreement between the temperature histories.

More efficient cooling mechanisms could be discussed later, such as thermoelectric coolers using the Peltier effect. Rowe [33] is a reference for the design and implementation of such device, while Lagoudas *et al.* [34] has made an attempt to use them in SMA actuators. However, the feasibility of such solutions is dismissed for the current application. Indeed, the amount of energy stored in the wires in the present application is be too important to allow such systems to be used. Noticeably, [34] deals with micro-actuators only. In addition, this reference uses SMA samples with partial recovery only, which is not satisfying. Those remarks underscore the drawbacks of using SMA to large scale applications. As a result of those investigations about alternative thermal control solutions, the cooling environment is assumed to be at most a reasonably forced air flow.

As a final comment on the models, it is important to note a serious weakness of SMA actuator design in general. No common behavior model has emerged yet that could be used as a reference model. In addition, no database is available for the characteristics of the alloys. More important still, no such energy-based model has been proposed that is simple enough to capture the main behavior of SMA, while being easily tractable to allow for a somewhat exhaustive design space exploration.

B.6 Placement of Actuators and Required End Stiffness

With local actuation, an important question to be answered is: what stiffness and displacement is required when the actuators are placed at given locations? A simple energy-based method to achieve the placement is presented here. We must say that this stiffness should be provided by the actuators, as we assume that the structure is very flexible ("smart skin").

Calling d_i the displacement of the structure at the actuator "i" and d the maximum deflection, we can write

$$E = \frac{1}{2}Kd^2 = \frac{1}{2}K_1 d_1^2 + \frac{1}{2}K_2 d_2^2 \tag{B.21}$$

We can estimate the displacement at the different locations from the beam equation. In addition, it is reasonable to have : $K_1 = K_2$. Thus we can solve for the stiffness, which leads to

$$K_1 = K_2 = \frac{K_{\text{req}}}{2f_1^2} \approx K \tag{B.22}$$

(in fact, we find $K_1 = K_2 = 0.934K$) Then, we can, through this method, translate the requirements given in terms of overall stiffness and displacements into requirements

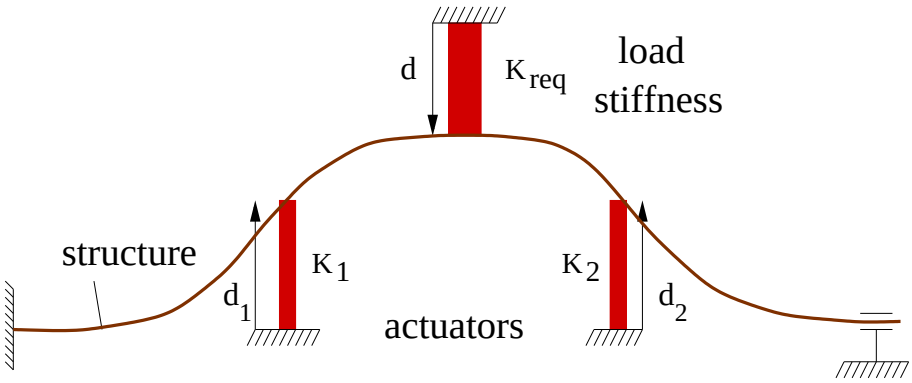

Figure B-2: Study of required stiffness of the actuators, in order to provide a required overall stiffness to the structure.

on the actuators. It should be noted that we assume the actuator stiffness to be all equal. More generally, we have to give a relation (convention: all equal) between the stiffnesses.

Appendix C

Nomenclature

We presents the nomenclature used in the thesis. The values or bounds are given when available, or comments are provided to explain the relationship between some of the variables.

Table C.1: Geometric description of the actuator.

θ	angle between SMAs and frames, which sets amplification ratio
l_s	length SMA wires, dummy variable before scaling
h	offset, computed from ls,θ
l_f	length of frames, computed from ls, h
A_s	cross-section area of SMA wires (total)
A_f	cross-section area of frames
D	diameter of SMA wires
n	number of wires required, computed from A_s, l_s, and D
K_end	end stiffness of the device
M_SMA	mass of SMA
M_tot	total mass of actuation device
A^*	ratio $\frac{A_\mathrm{s}}{A_\mathrm{f}}$ (mechanical efficiency)
K^*	ratio $\frac{K_\mathrm{s}}{K_\mathrm{f}}$ (impedance efficiency)

Table C.2: Material parameters.

E_a	Young's modulus of SMA - austenite, $E_\mathrm{a} = 90$ GPa
E_m	Young's modulus of SMA - martensite, $E_\mathrm{m} = 30$ GPa
E_s	Young's modulus of steel (frame and bias), $E_\mathrm{s} = 200$ GPa
ρ_{SMA}	density SMA, $\rho_{SMA} = 6500$ kg/m^3
ρ_s	density steel (frame and bias), $\rho_s = 7800$ kg/m^3

Table C.3: Shape memory effect.

ϵ	maximum strain in SMA, $\epsilon = 2\%$
T^0_{Ms}	martensite start temperature without load, $T^0_{\mathrm{Ms}} = 53$ C
T^0_{Mf}	martensite finish temperature, $T^0_{\mathrm{Mf}} = 36$ C
T^0_{As}	austenite start temperature, $T^0_{\mathrm{As}} = 46$ C
T^0_{Af}	austenite finish temperature, $T^0_{\mathrm{Af}} = 66$ C
T_{amb}	ambient temperature, $T_{\mathrm{amb}} = 35$ C
σ	stress in wires
C	transformation temperature - stress coefficient, $C = 7$ MPa/K
ΔH	latent heat of transformation, $\Delta H = 30$ kJ/kg
c_{p}	mass heat capacity, $c_{\mathrm{p}} = 250$ J/K/kg
C^0_{v}	heat capacity, $C^0_{\mathrm{v}} = 5.44 \times 10^{-6}\mathrm{J} \cdot \mathrm{K/m}^3$
h	free convection coefficient, $h = 30 - 40$ W/m^2/K
ρ	resistivity of SMA, $\rho = 102 \times 10^{-8}$ Ωm
R	resistance of the set of SMA wires
I	applied current to the wires, set to meet maximum available power
P	power available, $P = 300$ W or 2000 W maximum
J_{h}	heating time constant
J_{c}	cooling time constant (still air), $\times 10$ for forced convection
t_{h}	heating time
t_{c}	cooling time

References

[1] B.J. Janos. htpp://www.intellimat.com, 2000.

[2] S.J. Murray. Magnetic shape memory. Technical report, Material Processing Center, MIT - Materials Unlimited, May 1999.

[3] D.E. Hodgson, M.H. Wu, and R.J. Biermann. Shape memory alloys. Technical report, Shape Memory Applications,Inc., 1999.

[4] Hollerback, Hunter, and Ballantyne. *A Comparative Analysis of Actuator Technologies for Robotics*, cit. on http://amsl.mit.edu.

[5] A. Visconti, R. Fedeli, and A. Longhi. Aerodynamics drives chassis design on Ferrari 360 Modena. *SAE Technical paper series*, 2000.

[6] G. Lombardi, A. Vicere, H.G. Paap, and G. Manacorda. Optimized aerodynamic design for high performance cars. *AIAA-98-4789*, 1998.

[7] T.W. Duerig, K.N. Melton, D. Stockel, and C.M. Wayman. *Engineering Aspects of Shape Memory Alloy*. Butterworth-Heinemann, 1990.

[8] W. Huang. On the selection of shape memory alloys for actuators. *Materials and Design*, 23:11–19, 2002.

[9] M.F. Ashby. *Materials Selection in Mechanical Design (2nd edition)*. Butterworth-Heinemann, 1999. online at http://www.knovel.com/knovel2/.

[10] L.J. Garner, L.N. Wilson, D.C. Lagoudas, and O.K. Rediniotis. Devepopment of a shape memory alloy actuated biomimetic vehicle. *Smart Materials and Structures 9*, 2000.

[11] J.J. Epps and I. Chopra. In-flight tracking of helicopter rotor blades using shape memory alloy actuators. *Smart Materials and Structures 10*, 2001.

[12] D. Grant and V. Hayward. Design of shape memory alloy actuator with high strain and variable structure control. In *Procs. IEEE International Conference on Robotics and Automation, Cincinatti*, volume 3, pages 2305–2161, 1995.

[13] E. Makimo, T. Mitsuya, and T. Shibata. Fabrication of a NiTi shape memory micropump. *Sensors and actuators*, A 88:256–262, 2001.

[14] T.C. Waram. Actuator design using shape memory alloys. Technical report, Mondotronics,Inc., 1993.

[15] K Otsuka and C.M. Wayman. *Shape Memory Materials*. Cambridge University Press, 1998.

[16] X.D. Zhang, C. Liang, and C.A. Rogers. Modelling of two-way shape memory effect. *Intelligent Material Systems and Structures*, 8, 1997.

[17] M.A. Thrashert, A.R. Shahin, P.H. Meckl, and J.D. Jones. Efficiency analysis of shape memory alloy actuators. *Smart Materials and Structures 3*, 1994.

[18] Y. Tanaka. A thermomechanical sketch of shape memory effects: One-dimensional tensile behavior. *Res. Mechanica*, 18:251–263, 1986.

[19] A. Bekker and L.C. Brinson. Phase diagram based description of the hysteresis behavior of shape memory alloys. *Acta Mater.*, 46:3649–3665, 1998.

[20] B.J. de Blonk and D.C. Lagoudas. Actuation of elastomerics rods with embedded two-way shape memory alloy actuators. *Smart Materials and Structures 7*, 1998.

[21] Z. Bo, D.C. Lagoudas, and D. Miller. Material characterization of SMA actuators under non-proportional thermomechanical loading. *Engineering Materials and Technology*, 1998.

[22] L.C. Brinson and M.S. Huang. Simplifications and comparisons of shape memory alloy constitutive models. *Intelligent Materials and Structures 7*, 1996.

[23] S.G. Shu, D.C. Lagoudas, D. Hughes, and J.T. Wen. Modeling of a flexible beam actuated by shape memory alloy wires. *Smart Materials and Structures 6*, 1997.

[24] C. Liang and C.A. Rogers. Design of shape memory alloy actuators. *Mechanical Design*, 114:223–230, 1992.

[25] R. Stalmans and J. Van Humbeeck. Shape memory alloys: Functional and smart. presented in the seminar: 'Smart materials and technologies - sensors, control systems and regulators', Prague, Czech Republic, October 1995.

[26] A.J. Moskalik and D. Brei. Force-deflection behavior of individual unimorph piezoelectric C-block actuators. In *Procs. of the ASME Aerospace Division*, volume 52, pages 679–687, 1996.

[27] S.R. Hall and E.F. Prechtl. Development of a piezoelectric servoflap for helicopter rotor control. *Smart Materials and Structures 5*, 1996.

[28] E.F. Prechtl and S.R. Hall. Design of a high efficiency, large stroke, electromechanical actuator. *Smart Materials and Structures 8*, 1999.

[29] DARPA Boeing Phantom Works. SAMPSON project, http://www.darpa.mil/dso/thrust/md/smartmat/index.html.

[30] E.F. Prechtl. *Design and Implementation of a Piezoelectric Servoflap Actuation System for Helicopter Rotor Individual Blade Control*. Phd. thesis, MIT, Dept. Aeronautics and Astronautics, February 2000.

[31] E.M. Kasprzak, K.E. Lewis, and D.L. Milliken. Steady-state vehicle optimization using pareto-minimum analysis. *SAE Technical paper series*, 1998.

[32] Hansman Miller, DeWeck. Multifunctionality in parabolic RF antenna design based on SMA actuated radiation pattern shaping. *AIAA-98-4813*, 1998.

[33] D.M. Rowe. *CRC Handbook of Thermoelectrics*. CRC Press, 1994.

[34] A. Bhattacharyya, D.C. Lagoudas, Y. Wang, and V.K. Kinra. On the role of thermoelectric heat transfer in the design of SMA actuators: Theoretical modeling and experiment. *Smart Materials and Structures*, 4:252–263, 1995.

[35] TU Berlin. Adaptive airfoil with shape memory alloys. Online at http://www.thermodynamik.tu-berlin.de/haupt/fluegel/transition.html.

[36] S. Hirose, K. Ikuta, and Y. Umetani. Development of shape memory actuators. performance assessment and introduction of a new composing approach. *Advanced Robotics*, 3, No. 1:3–16, 1989.

[37] C. Liang and C.A. Rogers. One-dimentional thermomechanical constitutive relations for shape memory materials. *Intelligent Materials and Structures 1*, 1990.

[38] Y. Matsuzaki, H. Naito, T. Ikeda, and K. Funami. Thermo-mechanical behavior associated with pseudoelastic transformation of shape memory alloys. *Smart Materials and Structures*, 10:884–892, 2001.

[39] V. Brailovski, F. Trochu, and A. Leboeuf. Design of shape memory linear actuators. In *SMST-97, Asilomar, CA, USA, March 2-6 1997*, 1997.

[40] V. Giurgiutiu and C.A. Rogers. Incrementally adjustable rotor-blade tracking tab using SMA composites. In *Procs. of the 38th AIAA/ASME/ASCE/AHS/ASC Structures, Structural Dynamics, and Materials Conference, and Adaptive Structures Forum, Kissimmee, FL, April 7-10 1997, paper #97-1387*, 1997.

[41] G.V. Webb, D.C. Lagoudas, and M. Kulkarni. Adaptive shape control for an SMA-actuated aerofoil rib structure. In *Procs. of IMCE'99, ASME International Mechanical Engineering Congress and Exposition, November 14-19, 1999, Nashville, Tennessee*, 1999.

[42] Th. Bein, H. Hanselka, and E. Breitbach. An adaptive spoiler to control the transonic shock. *Smart Materials and Structures*, 9:141–148, 2000.

[43] O.K. Rediniotis, D.C. Lagoudas, L.J. Garner, and N. Wilson. Experiments and analysis of an active hydrofoil with SMA actuators. *AIAA Paper 98-0102*, 1998.

[44] D. Salle. Design of a robotic arm, actuated by shape memory alloys. In *Procs. IEEE Canadian Conference on Electrical and Computer Engineering, Edmonton, Alberta, Canada, May 9-12 1999*, 1999.

[45] Y. Tanaka and A. Yamada. A rotary actuator using shape memory alloy for a robot - analysis of the response with load. In *IEEE/RSJ International workshop on intelligent robots and systems IROS'91, Nov. 3-5 1991, Osaka, Japan*, 1991.

[46] R. Barrett and R.S. Gross. Super-active shape-memory alloy composites. *Smart Materials and Structures*, 5:255–260, 1996.

[47] U. Icardi. Large bending actuator made with SMA contractile wires: Theory, numerical simulation and experiments. *Composites, part B*, 32:259–267, 2001.

[48] D.A. Hebda and S.R. White. Effect of training conditions and extended thermal cycling on nitinol two-way shape memory behavior. *Smart Materials and Structures*, 4, 1995.

[49] D.A. Miller and D.C. Lagoudas. Thermomechanical characterization of NiTiCu and NiTi SMA actuators: Influence of plastic strains. *Smart Materials and Structures 9*, 2000.

[50] L.C. Brinson, Huang, Boller, and Brand. Analysis of controlled beam deflection using SMA wires. *Intelligent Material Systems and Structures, vol 8 #1*, 1997.

[51] G. Song, B. Kelly, and B.N. Agrawal. Active position control of a shape memory alloy wire actuated composite beam. *Smart Materials and Structures 9*, 2000.

[52] S. Choi and J.J. Lee. The shape control of a composite beam with embedded shape memory alloy wire actuators. *Smart Materials and Structures 7*, 1998.

[53] S. Seelecke and C. Buskens. Optimal control of beam structures by shape memory wires. In *Proceedings of the OPTI 97, Computer Aided Optimum Design of Structures V, September 8 -10, 1997, Rome, Italy , Comp.Mech. Press*, 1997.